https://doi.org/10.5194/egusphere-2026-2858
Preprint. Discussion started: 10 June 2026

How hidden variables limit the performance of shallow landslide susceptibility models

Tobias Halter[1,2,3,4], Manfred Stähli[1], Alexander Bast[2,3], Peter Lehmann[5] and Jordan Aaron[4]

[1]Swiss Federal Institute for Forest, Snow and Landscape Research WSL, Zürcherstrasse 111, 8903 Birmensdorf, Switzerland
[2]WSL Institute for Snow and Avalanche Research SLF, Flüelastrasse 11, 7260 Davos Dorf, Switzerland
[3]Climate Change, Extremes and Natural Hazards in Alpine Regions Research Centre CERC, Flüelastrasse 11, 7260 Davos Dorf, Switzerland
[4]Department of Earth Science, ETH Zurich, Sonneggstrasse 5, 8092 Zürich, Switzerland
[5]Department of Environmental Systems Science, ETH Zurich, Universitätstrasse 16, 8092 Zürich, Switzerland

Correspondence to: Tobias Halter (tobias.halter@wsl.ch)

Abstract

Susceptibility mapping is critical in assessing shallow landslide hazard and sediment transport potential. Advancements in modelling techniques and the availability of high-resolution spatial data have continuously improved the performance of landslide susceptibility maps. Nevertheless, discrepancies between predicted susceptibility and observed landslide occurrence remain. In addition to shortcomings in model design and the incompleteness of landslide inventories, the accuracy and transferability of susceptibility models are critically limited by hidden variables, such as site-specific variability in soil development, that control the triggering process but are rarely available in inventories. Here we developed an extensive case study framework, and apply it to two uniquely detailed inventories in order to quantify the role of hidden variables, as well the effects of incomplete landslide inventories. The first inventory is a comprehensive regional dataset containing over 24,000 mapped landslides across 5,939 km², and the second is a field-validated dataset of 734 landslides which includes detailed documentation of hidden variables. We trained two Random Forest machine learning models using a wide range of explanatory variables, including topography, land cover, soil properties, and climate. The first model was optimized for the first dataset, and achieved high predictive performance within its training domain (mean cross-validation of the area under the curve, AUC = 0.89). However, its accuracy decreased significantly (AUC = 0.74) when applied to the second dataset, highlighting limitations in transferability. The second model was optimized for the second dataset (AUC = 0.79). A comparison of the two models revealed that regional climatic and geologic data hindered transferability to remote regions because the relationship between available and hidden variables is not properly captured by the susceptibility model. We further analysed the predicted susceptibility values as a function of the site-specific information collected in the second database, to quantitatively explore the role of hidden variables. The analysis suggested that variables related to (i) subsurface heterogeneity and (ii) vegetation complexity govern landslide initiation, but are rarely accounted for in susceptibility models. Specifically, the models underestimated susceptibility in poorly developed soils and areas with uniform forest layering. This study underscores the necessity of a process-based understanding grounded in field observations to capture the full complexity of landslide failure mechanisms, relevant to landslide susceptibility modelling.

https://doi.org/10.5194/egusphere-2026-2858
Preprint. Discussion started: 10 June 2026

1 Introduction

Shallow landslides fail along shallow slip surfaces of less than 2 m depth. Through the mobilization of sediment material, they act as important agents of hillslope erosion and contribute to the evolution of mountainous landscapes (Sidle and Ochiai, 2006; Burton and Bathurst, 1998). Shallow landslides cause significant damage and loss of life as their initiation locations are difficult to predict, and they can emplace with extremely rapid velocities (Hungr et al., 2014). Shallow landslides commonly initiate on steep slopes, particularly during intense rainfall or earthquake events (Baum and Godt, 2010). They may further evolve into destructive debris flows (Gabet and Mudd, 2006), which represent some of the most hazardous mass movement processes worldwide (Hong et al., 2007). To support hazard management and estimate sediment transport potential, susceptibility maps have emerged as essential tools (Fell et al., 2008), aiming to predict the spatial deposition of slope failure across a landscape (Corominas et al., 2014). Despite the substantial progress in improving the quality of susceptibility predictions across various fields of research, landslides continue to occur at unexpected locations, resulting in damage to infrastructure and buildings, loss of life. Understanding the reason for these limitations is critical to improving susceptibility mapping, but has been hindered by a lack of site specific data on sufficient spatial scales needed to quantify the physical mechanisms typically missed by current approaches. The present study uses two unique datasets to overcome this limitation.

State of the art susceptibility assessments are typically based on either physically (deterministic) or data-driven (probabilistic) models (Shano et al., 2020). Physically based models aim to reproduce slope failure processes by coupling subsurface hydrological flow with mechanical stability analyses (Montgomery and Dietrich, 1994; Rossi et al., 2013). Applied to regional scale, they are often limited by scarce information about the heterogeneity of hydrological and mechanical properties of the subsurface (Godt et al., 2008). Data-driven models correlate observed landslide locations with spatial explanatory variables, assuming that future landslides will be governed by the same factors as the observed landslides (van Westen et al., 2008). Such analyses commonly incorporate a wide range of explanatory variables, including morphology, climatic, pedologic, geologic, and land-use factors (Ado et al., 2022; Zhao et al., 2023). Advances in remote sensing have substantially improved the quality and spatial resolution of input data. Airborne laser scanning, for example, enables detailed mapping of terrain and vegetation, producing high-quality digital elevation models (DEMs) and digital surface models (Ginzler et al., 2019; Liu, 2008; Swisstopo 2025a). Combined with monitoring and modelling approaches, spatial datasets of climate and soil properties can be derived (Karger et al., 2017; Ma et al., 2019). In addition, satellite-based remote sensing provides global-scale Earth observation data, supporting the assessment of vegetation indices and land-cover information (Huang et al., 2024; Defries and Townshend, 1999). Despite performance improvements resulting from the increasing availability of spatial geodata, large landslide inventories, and advances in machine learning algorithms (Merghadi et al., 2020; Ado et al., 2022), landslide susceptibility models remain inherently imperfect.

Although many studies have investigated individual sources of model imperfection (described in detail in the next section), no study has systematically summarized and quantified the effect of these limitations on model performance. To address this, we investigate the main sources of model uncertainty using two susceptibility models trained and tested on two comprehensive

https://doi.org/10.5194/egusphere-2026-2858
Preprint. Discussion started: 10 June 2026

landslide inventories from Switzerland. To do this, we first summarize the main sources of uncertainty and then give an overview of the datasets and methods we use to investigate them. We then present the results obtained using the two susceptibility models and discuss them in the context of the most important uncertainties when constructing data-driven susceptibility models.

2 Background

In landslide research, individual sources of model imperfection have been studied in detail and can be categorized into four primary groups: (a) limitations related to the model design, (b) limitations caused by incomplete landslide inventories, (c) limitations related to the transferability of models to unseen data, and (d) limitations arising from explanatory variables that cannot fully represent the environmental complexity controlling slope instability.

The first group (a) includes modelling choices such as the selection of algorithms used to classify landslide susceptibility. Common approaches in data-driven susceptibility modelling include linear and logistic regression (e.g., von Ruette et al., 2011; Zweifel et al., 2021; Edrich et al., 2023), as well as machine learning algorithms such as Random Forest (Taalab et al., 2018; Kim et al., 2018), support vector machines (e.g., Pourghasemi et al., 2013), artificial neural network (e.g., Ermini et al., 2005; Kavzoglu et al., 2021) and hybrid modelling approaches (Nguyen et al., 2019; Jaafari et al., 2019). With increasing data availability and improved computational methods, many studies have shown that machine learning approaches often outperform common statistical models in landslide susceptibility classification (Huang et al., 2020; Goetz et al., 2015; Akinci and Zeybek, 2021). Among machine learning based methods, studies report that classification tree-based methods, such as Random Forest models are best at discriminating landslide susceptibility (Merghadi et al., 2020; Chicas et al., 2024; Liu et al., 2023; Pourghasemi and Rahmati, 2018; Sun et al., 2023; Goetz et al., 2015). Beyond algorithm selection, landslide susceptibility mapping is sensitive to model design regarding the choice of mapping units and their resolution (Guzzetti, 2006; Erener and Düzgün, 2012). While raster-based mapping remains a popular choice due to its straightforward integration with geographical information system (GIS) data, such as DEMs or their derivatives, slope-unit-based mapping provides a more physically meaningful framework by capturing actual landslide geometries and the environmental conditions driving slope failure (Ba et al., 2018; Sun et al., 2023). The performance of these models is further dictated by the resolution of the units, as inappropriate sizes of grid cells or slope-units can fail to accurately represent the specific conditions relevant to landslide initiation (Karsa et al., 2019; Lee et al., 2004; Palamakumbure et al., 2015). This sensitivity extends to the sampling strategies used to define triggering and non-triggering areas used for modelling (Gu et al., 2024; Lai et al., 2019; Hong et al., 2019; Hong et al., 2024).

Furthermore, the reliability of these data-driven assessments is limited by the quality of the landslide inventory itself (Huang et al., 2024; Titti et al., 2021; Mirus et al., 2020; Woodard et al., 2023). Systematic inventory incompleteness (b), often a byproduct of the acquisition method, introduces critical errors where missed landslides are incorrectly categorized as non-landslide samples, thereby reducing the model's ability to discriminate between stable and unstable terrain (Steger et al., 2017;

https://doi.org/10.5194/egusphere-2026-2858
Preprint. Discussion started: 10 June 2026

van Westen et al., 2008). Similarly, inaccurate positioning of mapped landslides constrain the model's capacity to represent actual environmental drivers of landslide susceptibility (Steger et al., 2016b).

Limitations in spatial transferability (c) to unseen data is central to susceptibility mapping (Zhu et al., 2020), as a model's ability to generalize across independent regions is a relevant benchmark of its quality (Chung and Fabbri, 2003). In a standard machine learning workflow, datasets are typically partitioned into training, validation, and test sets. The training set fits the model, the validation set optimizes input features and hyperparameters, and the test set provides an unbiased evaluation of performance on geographically distinct data (Ripley, 2007). Previous studies have shown that limited spatial transferability may result from small training sample sizes (Petschko et al., 2014), incomplete landslide inventories (Steger et al., 2017) or incomplete explanatory data (Woodard et al., 2023). However, the specific role of individual environmental variables in hindering transferability remains poorly understood.

Susceptibility assessments are further limited by the inherent incompatibility of explanatory variables to represent the heterogeneity of environmental conditions relevant to slope instability (d). Despite advancements in high-resolution remote sensing, current datasets primarily capture surface or near-surface conditions, failing to account for subsurface heterogeneity such as the spatial variability in soil properties, soil depth, and bedrock topography which exert first-order controls on where landslides initiate within the landscape (Fan et al., 2016; Moradi et al., 2018; Lanni et al., 2013). These studies on such first-order controlling factors are largely based on physical modelling and often lack empirical field observations of the required resolution. Moreover, these models typically do not represent complex soil structural features (Fusco et al., 2021) like soil macropores and fractures, formed by biological, physical, or chemical processes that can induce preferential flow (Beven and Germann, 1982). Such structures may either enhance stability through improved drainage or promote instability when flow networks become oversaturated, leading to increased pore-water pressure in the surrounding soil matrix (Uchida et al. 2001; Uchida 2004). Additional processes, including lateral water flow along the soil–bedrock interface (McDonnell, 2003), bedrock connectivity (Kosugi et al., 2006) and bedrock exfiltration (Brönnimann et al., 2013), further increase the complexity of subsurface hydrological controls on slope stability. Vegetation enhances slope stability through mechanical root reinforcement (Roering et al., 2003; Schwarz et al., 2011) and by influencing hydrological processes, including preferential flow, interception, evapotranspiration, and hydraulic conductivity, thereby affecting pore-water pressure dynamics (Ghestem et al., 2011; Graf et al., 2017). In forested systems, these effects are further controlled by forest structure, such as canopy cover and vertical layering, which regulate both hydrological processes and root reinforcement (Rickli et al., 2019; Bast et al., 2026). However, most susceptibility models still represent vegetation in a highly simplified manner due to constraints in large-scale data availability and resolution (Franklin, 1995; Bast et al., 2025), typically as presence–absence or land-cover classes (Piacentini et al., 2012; Neuhäuser et al., 2012), and rarely account for plant species-specific traits or forest structural characteristics relevant to slope stability (McGuire et al., 2016; Rickli et al., 2019).

https://doi.org/10.5194/egusphere-2026-2858
Preprint. Discussion started: 10 June 2026

3 Material and Methods

We have designed our study and selected datasets in order to quantify the importance of three of the four types of model limitations described above. Model design limitations (a) were not examined in detail and were instead addressed through a structured study design informed by literature. Two comprehensive landslide inventories from Switzerland were used to train and test two different susceptibility models. In the first model (independent model), the landslide inventory from the canton of Bern, featuring more than 24'000 landslides was used for training and validation (model optimization), while the Shallow Landslide Database (SLD) featuring 734 landslides from diverse geographic regions of Switzerland served as an independent test dataset. In the second model (dependent model), the Bern inventory data was again used for training, but this time the SLD was used for both validation and testing, allowing information from the test dataset to influence model optimization. Performance comparison between the two inventories allowed to assess the effect of landslide inventory incompleteness (b). Transferability limitations (c) were quantified by analysing the performance of the independent model on the test data and by comparing the selected explanatory variables between the two models. Subsequently, susceptibility predictions of both models were compared to specific field-based observations from the SLD that cannot be represented at regional scale (termed "hidden variables"). False negatives, i.e. landslides occurring at locations predicted with low susceptibility and under systematic conditions linked to hidden variables highlighted fundamental limitations in how models represent predisposing conditions based on available explanatory variables (d). The landslide inventories, as well as the model training procedure, are described in detail in the following sections.

3.1 Landslide inventories

3.1.1 Canton Bern

The landslide inventory of the Canton of Bern, compiled by Hählen (2024), includes 24,024 landslides. Of these, 19,895 were manually mapped at the release area centre using orthophotos from 1962 to 2021. The orthophotos have a ground resolution of 10 – 25 cm and were updated every three years; images prior to 1998 were available at 50 cm resolution and were updated every five years (Swisstopo, 2025c). The dataset was further supplemented by an event register of the Canton of Bern, adding 4,129 additional landslide records (Hählen, 2024). Visual quality control indicated high positional accuracy of the mapped landslides. However, the degree of inventory incompleteness could not be quantified, particularly for landslides where deposits have been removed between orthophoto acquisitions or for landslides occurring in forests where vegetation may obscure geomorphic evidence (van Westen et al., 2008).

The Canton of Bern is a suitable region for capturing the geographical heterogeneity of Switzerland due to the pronounced diversity in topographic, geological, climatic, and ecological conditions. It is the second-largest canton in Switzerland, covering an area of 5,939 km² and extending from the Jura Mountains in the north, across the Swiss Plateau, to the Alps in the south (Fig. 1). Elevation ranges from 399 m a.s.l. to 4,273 m a.s.l. Mean annual precipitation increases with altitude, from approximately 1,000 – 1,300 mm on the Swiss Plateau to about 2,500 mm in the Bernese Alps (MeteoSwiss, 2024). The

https://doi.org/10.5194/egusphere-2026-2858
Preprint. Discussion started: 10 June 2026

dominant lithologies include Jurassic limestone in the Jura Mountains; sedimentary rocks such as marl, conglomerate, and sandstone of the Molasse Basin in the Swiss Plateau; and limestone of the Helvetic nappes as well as plutonic and metamorphic
165 rocks of the crystalline basement in the Bernese Alps.

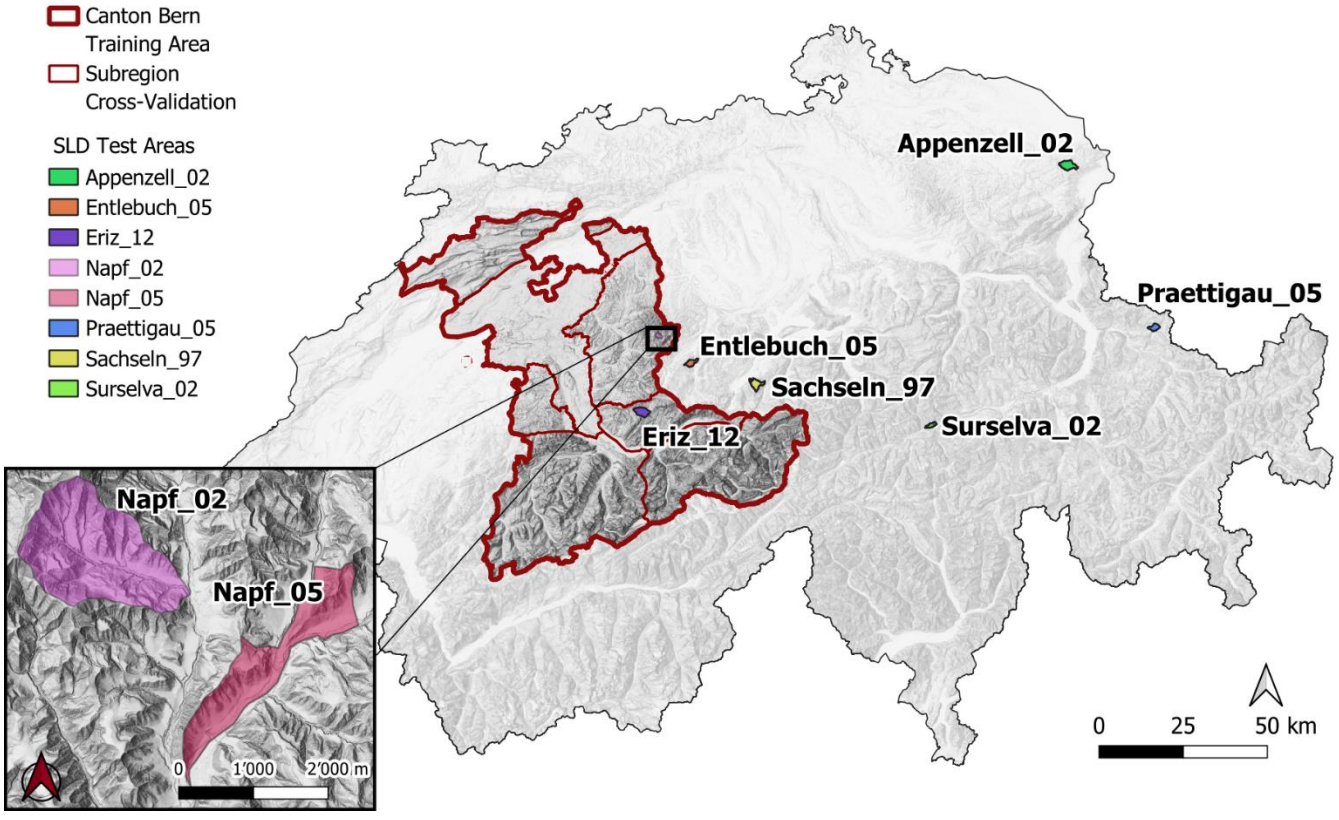

Fig. 1. Map of Switzerland highlighting the training area, i.e. the Canton of Bern. The seven geographical subregions (Hählen, 2024) are used for spatial cross-validation (red thin lines). The eight coloured regions correspond to the perimeters of the Shallow Landslide Database (SLD). Labels denote the regional names and the year of the landslide triggering rainfall event.

170 3.1.2 Shallow Landslide Database (SLD)

The Shallow Landslide Database (SLD; Rickli et al., 2016) is a unique dataset that allowed to quantify model transferability, and assess the role of hidden variables in susceptibility model performance. This event-based dataset has been compiled over the past 30 years from detailed field observations following heavy rainfall events associated with numerous shallow landslides. For each event, a perimeter was defined and all landslides with volumes exceeding 30 m³ were documented. In total, 734
175 landslides were recorded across eight perimeters located in the northern and eastern Swiss Alps (Fig. 1), three of which are located within the Canton of Bern. To ensure independent testing, these three perimeters were only used for the test and excluded for model training. The documented landslides vary widely in size, ranging up to 2,600 m², with a median area of 135 m². Of the total landslides, 407 occurred outside forested areas and 327 within forests. As the SLD inventory records only

https://doi.org/10.5194/egusphere-2026-2858
Preprint. Discussion started: 10 June 2026

the coordinates of the uppermost point of each landslide (head scarp), centroids and release areas were approximated using elliptical polygons based on reported release area, maximum length, maximum width, and slope aspect.

3.2 Commonly used Explanatory Variables

To train the susceptibility models, we considered a wide range of topographic, morphologic, climatic, pedologic, geologic and land-use explanatory variables (Table 1) that are commonly found in landslide susceptibility analyses (Ado et al., 2022; Chicas et al., 2024; Zhao et al., 2023). It should be noted that these variables were considered static, ignoring the fact that environmental conditions are constantly changing. A landslide may have occurred before or after the data was acquired. In the following, all 33 variables are described, together with their primary contributions to landslide susceptibility. Where direct spatial input data were unavailable, variables were derived using SAGA (Conrad et al., 2015), GDAL (GDAL/OGR contributors, 2025), QGIS (Dawson et al., 2025) and GRASS (GRASS Development Team, 2024) tools within QGIS (Table 1).

3.2.1 Topographical & Morphological variables (9 variables)

Topographic and morphologic attributes were derived from a high-resolution (2 m) digital elevation model (DEM) provided by Swisstopo (2025a). *Elevation* was included as an explanatory variable to represent climatic controls on vegetation and soil types through variations in weathering rates (Egli et al., 2008). *Slope gradient* was computed as the maximum elevation gradient between neighbouring cells. Slope is widely regarded as a key variable representing gravitational forces acting within the subsurface (Budhu, 2015), and controls the availability of unconsolidated material susceptible to shallow landslide initiation (Moser, 1997).

Aspect was transformed using a cosine function such that values of 0 represent north-facing slopes and values of 1 represent south-facing slopes, with intermediate aspects varying continuously. Aspect captures spatial variability in solar radiation, which influences hydrological and climatic conditions relevant to vegetation growth and slope stability (Gutiérrez-Jurado and Vivoni, 2013). *Flow accumulation* was computed considering sink filling by Wang and Liu (2006) and a multiple flow direction algorithm (Conrad et al., 2015). Flow accumulation represents the contributing upslope area draining into each raster cell and serves as a proxy for water accumulation within slopes. *Planform curvature* describes the concave (negative) or convex (positive) shape of a slope perpendicular to the direction of maximum gradient, whereas *profile curvature* describes curvature parallel to the slope direction. Planform curvature influences the convergence and divergence of surface flow, while profile curvature governs flow acceleration and deceleration (Zevenbergen and Thorne, 1987). *General curvature* represents the mean of planform and profile curvature and reflects overall surface bending. Topographic wetness index (*TWI*) was defined as the natural logarithm of the upslope contributing area divided by the tangent of the local slope, whereas Topographic Position Index (*TPI*) was calculated as the elevation difference between a cell and the mean elevation of its surrounding neighbourhood. To adequately capture the surface roughness and geomorphological landforms relevant to slope stability, the neighbouring

https://doi.org/10.5194/egusphere-2026-2858
Preprint. Discussion started: 10 June 2026

area of consideration for the computation of the TPI was set to 3 x 3 surrounding grid cells (Neuhäuser et al., 2012; Piacentini et al., 2015). Together with curvature measures, TWI and TPI were included as explanatory variables to represent topographic controls on surface and subsurface hydrological flow paths (Nohani et al., 2019), as well as mechanical stresses acting within the subsurface.

3.2.2 Vegetation variables (3 variables)

To account for vegetation effects on slope stability, we incorporated a Swiss *vegetation height* map (Ginzler, 2023) and a national annual mean Normalized Difference Vegetation Index (*NDVI*) dataset (UniGeneva, 2019). In addition, raster cells were classified as *forest* when the minimum vegetation height exceeded 5 m (Unesco, 1973), while cells with lower vegetation height were classified as non-forest. Vegetation height serves as a proxy for root biomass and rooting depth (Heisse et al., 2007), influencing slope stability through mechanical root reinforcement (Schwarz et al., 2011) and hydrological effects such as increased evapotranspiration. *NDVI*, in turn, reflects vegetation density and land-use characteristics (Dahigamuwa et al., 2016).

3.2.3 Geological variables (3 variables)

To account for geological conditions affecting slope stability, we used the national GeoCover dataset (Swisstopo. 2025b) and extracted the *main geological classes*, which categorize the landscape into: (1) Quaternary unconsolidated material, (2) sedimentary rocks, (3) magmatic rocks, (4) metamorphic rocks, and (5) lakes and glaciers. Because shallow landslides predominantly occur in unconsolidated materials, this subclass was further subdivided—while retaining the other subclasses—into moraine, loess, loamy colluvium, gravelly colluvium, river gravel, and alluvium, based on GeoCover information, and included as an additional variable (*mixed geological classes*).

Classification is relevant for slope stability analyses because landslides may initiate either within bedrock, within the soil or at soil–bedrock interfaces, depending on mechanical and hydrological properties (Clarke and Burbank, 2011), and because bedrock lithology influences soil properties through weathering processes (Blume et al., 2016). In addition, *hydrogeological classes* from the same dataset were incorporated, classifying areas into different productivities of ground water resources. Hydrogeology influences slope stability by regulating infiltration, subsurface flow, and exfiltration between soil and bedrock (Onda et al., 2001). Although more detailed lithological and tectonic information is available in the GeoCover dataset, these variables were excluded because some categories are present only in the test dataset and not in the training dataset, which would prevent consistent model application.

3.2.4 Climate variables (10 variables)

Climatic variables were derived from the CHELSA dataset and include *mean annual snow cover duration*, potential evapotranspiration *(PET),* plant *growing season length*, and *frost change frequency* (Karger et al., 2017). Mean *annual temperature* and *precipitation* were obtained from a Daymet product (Thornton et al., 1997) based on MeteoSwiss observations

https://doi.org/10.5194/egusphere-2026-2858
Preprint. Discussion started: 10 June 2026

for the period 1981–2010 (MeteoSwiss, 2024). Climatic variables capture local and regional differences that influence shallow landslide susceptibility through their effects on vegetation, soil formation, and landscape evolution (Persichillo et al., 2017; Perron, 2017), as well as hillslope adaptation to rainfall intensity and frequency (Leonarduzzi and Molnar, 2020). To explicitly account for extreme rainfall conditions, spatial datasets of maximum rainfall intensity over 60-minute *(Prec_60min_30y)* and 24-hour *(Prec_24h_30y)* durations with a 30-year return period were included (Fukutome et al., 2023). As additional variables, we normalized these values by dividing them by the local mean annual precipitation *(Prec_60min_30y_per_mean* and *Prec_24h_30y_per_mean).*

3.2.5 Soil variables (5 variables)

Soil properties were represented using soil texture maps from KOBO (2024), which provide *sand*, *silt*, and *clay content* for three depth intervals (0–30, 30–60, and 60–120 cm). To reduce dimensionality, depth-weighted mean values for each texture fraction were computed across the full soil profile. *Bulk density* was derived as a weighted mean from SoilGrids maps (Poggio et al., 2021), available for six depth intervals (0–5, 5–15, 15–30, 30–60, 60–100, and 100–200 cm). Soil texture and bulk density influence both hydrological and mechanical soil properties relevant to slope stability (Fredlund and Rahardjo, 1993). In addition, *soil depth* was estimated using the sGIST approach (Catani et al., 2010), which relates soil thickness to slope gradient, profile curvature, and relative elevation within the contributing catchment. Topographic inputs for the soil depth mapping were derived from the downscaled SwissALTI3D DEM (Swisstopo 2023a), and catchments were delineated using HydroBASINS Level 8 sub-basins (Lehner and Grill, 2013). Soil depth affects shear and effective stresses along potential failure planes (Terzaghi, 1943) and controls soil water storage capacity and saturation dynamics (Lu and Godt, 2013).

3.2.6 Proximity variables (3 variables)

Proximity variables were obtained from the national topographic landscape model swissTLM3D (Swisstopo, 2025d), which contains more than 21 million mapped objects. Mapped roads and paths as well as waterways were used to compute the distance from each raster cell to the *nearest road* or *nearest stream* with the base QGIS vector tools “join attributes by nearest”. Distance to the nearest stream may illustrate the hydrological properties and saturation characteristics of the terrain (Lima et al., 2022). Areas intersecting roads or paths were additionally classified with the binary *road* variable. Distance to roads is commonly included in susceptibility analyses because landslides are often preferentially documented near roads (van Westen et al., 2008). Although this bias is not expected in our study due to comprehensive orthophoto-based mapping, roads may still influence slope stability through excavation, embankments, and altered drainage pathways (Guadagno et al., 2005). Roads can concentrate surface runoff and redirect water into hillslopes, thereby increasing localized subsurface infiltration (Montgomery, 1994).

Table 1. Overview of explanatory variables used for the susceptibility analyses, including the variable type, the original resolution of the data (before up-/downscaling), the tool used to compute the variable and the source of the variables. TWI stands for Topographic Wetness Index, TPI for Topographic Position Index, NDVI for Normalized Difference Vegetation Index and PET for potential evapotranspiration rate. Prec_60min_30y and Prec_24h_30y stand for extreme precipitation events with a return period

https://doi.org/10.5194/egusphere-2026-2858
Preprint. Discussion started: 10 June 2026

of 30 years in durations of 60 minutes or 24 hours, respectively; and Prec_60min_30y_per_mean as well as Prec_24h_30y_per_mean for these attributes divided by mean annual precipitation. The 'x' in Model 1 and Model 2 indicates if a variable was used in the independent model (here called Model 1) or the dependent model (here denoted as Model 2)

Explanatory variable	Model 1	Model 2	Type	Resolution	Tool	Source
Elevation	x		Numerical	2 m	-	SwissALTI3D (Swisstopo, 2025a)
Slope gradient	x	x			GRASS Development Team (2024)	
Aspect	x	x				
TWI	x	x				
Flow accumulation	x	x			SAGA GIS (Conrad et al., 2015)	
Curvature profile	x	x				
Curvature planform	x	x				
Curvature general	x	x				
TPI	x	x			(GDAL/OGR contributors, 2025)	
Vegetation height	x	x	Numerical	10 m	-	Ginzler (2023)
Forest	x		Category		> 5 m height	
NDVI	x	x	Numerical	26 m x 38 m	-	UniGeneva (2019)
Main geological classes	x		Category	Polygon shapefile	-	Geocover (Swisstopo, 2025b)
Mixed geological classes	x					
Hydrogeological classes	x					
Snow cover days	x	x	Numerical	~1000 m	-	CHELSA (Karger et al., 2017)
Mean PET	x					
Frost change frequency	x					
Growing season length		x				
Mean precipitation				100 m		Daymet (MeteoSwiss, 2024)
Mean temperature		x		100 m		
Prec_60min_30y	x	x		1000 m		Hydromaps (Fukutome et al., 2023)
Prec_24h_30y	x	x				
Prec_60min_30y_per_mean	x					
Prec_24h_30y_per_mean	x					
Sand content			Numerical	90 m	-	KOBO (2024)
Silt content		x				
Clay content	x	x				
Bulk Density	x			250 m	-	Soil Grids (Poggio et al., 2021)
Soil depth	x	x		2 m	sGIST (Catani et al., 2010)	SwissALTI3D (Swisstopo, 2025a)
Road			Category	Line Shapefile	-	swissTLM3D (Swisstopo, 2025d)
Distance to nearest road	x		Numerical		join attributes by nearest (Dawson et al., 2025)	
Distance to nearest stream	x	x				

3.3 Hidden Explanatory Variables

To explore the role of hidden variables, i.e. those that cannot currently be represented accurately at a regional scale, we took advantage of the detailed field mapping presented in the SLD inventory. This inventory provides comprehensive information

https://doi.org/10.5194/egusphere-2026-2858
Preprint. Discussion started: 10 June 2026

on landslide dimensions, land use, local hydrology, soil profiles, bedrock depth, as well as geomorphology and vegetation characteristics that are much more detailed than provided in existent maps. For the purposes of this study, text-based variables used in the inventories (e.g. “brown earth over bedrock”) were simplified and converted into categorical variables (e.g. “brown earth”) through keyword extraction. Variables documented for fewer than 100 landslides and individual categories of these variables with less than 10 landslides were excluded to ensure a statistically sufficient sample size. Additionally, regional specific information, such as lithology and tectonic setting were omitted, as they only vary between the eight SLD perimeters and are therefore irrelevant to explain variations at small scales.

In total, 23 categorical variables were retained to characterize the landslide environment (Table 2). Four variables were derived from soil profiles. *Soil types* were classified in the inventory according to the guidelines of the German Soil Science Society. The four soil types found in the inventory with at least 10 landslides—Brown Earth, Regosol, Rendzina, and Pseudogley—correspond to the World Reference Base for Soil Resources classes Cambisol, Regosol, Leptosol, and Albeluvisol, respectively (Schad, 2023). Based on this classification, information on *soil development* was inferred. Poorly developed (raw) soils were defined as soils lacking a developed B horizon such as Regosol and Rendzina, while Brown Earth correspond to developed soils and Pseudogly to wet soils (Rickli et al., 2016). Poorly developed soils are typically either relatively young or have experienced inhibited development due to erosion or depositional processes, rockiness, or anthropogenic disturbances such as agriculture, logging, or litter removal (Blume et al., 2016; Duchaufour, 1982). Additional to the pedological soil type characterisation, soils were classified visually according to the Unified Soil Classification System class (*USCS class).* To integrate information on macropores, we defined a composite variable (*macropores presence*), classifying soils as: (1) *no macropores* – when no old root channels, soil fractures, mouse channels, or worm channels were observed; (2) *few macropores* – when pores were observed in one of the above named macropore classes; and (3) *many macropores* – when pores were observed in more than two classes.

Eight variables characterize the vegetation in the surrounding area (100 x 100 m around the release area, Rickli et al., 2016). *Vegetation habitat* distinguishes between mesic, alternating moist and alternating mesic conditions. *Meadow use intensity* and *meadow type* (meadow or pasture) describe the agricultural use of vegetation of landslides occurring outside forests. Forest characteristics include *forest mixture* differentiating between coniferous and deciduous forests, *forest canopy cover* classifying the percentage of canopy coverage, and *forest condition* indicating damage from windthrow, bark beetles, or wildfire. *Forest development* classifies stands by dominant tree diameter, while *forest layering* describes vertical structural diversity. To simplify this variable, structurally complex forests were merged with multi-layered forests resulting in the two classes single-layered and multi-layered forests (Bast et al., 2025)

Three variables describe the landslide process, including whether the movement was translational or rotational (*landslide mechanism*), whether it occurred as *a flow or slide process*, and the position of the failure plane within the soil profile (*slide plane interface*). Two variables describe the hydrological conditions, with indication about the *amount of water flowing* at the time of field documentation as well as the overall *wetness of the site*. One variable characterizes the morphological setting of each landslide location, distinguishing between convex and concave terrain in both the horizontal and vertical slope directions

https://doi.org/10.5194/egusphere-2026-2858
Preprint. Discussion started: 10 June 2026

(*morphological class*). Three variables describe previous landslide activity in the surrounding area, including whether landslides are still visually detectable (*signs old slides*), if surrounding landslides occurred less than ten years ago (*signs recent slides*), and the observed intensity of nearby occurrences (*intensity previous slides*). Two variables capture geological information: one indicates the presence of *interbedded rock layers*, and the other documents the interpreted *geological soil unit*.

Table 2. Overview of hidden variables from the shallow landslide database (SLD) used in the analysis. All variables are categorical variables describing local properties that may be relevant to slope stability.

Hidden variable name	Categories and number of samples per category (n)	Variable domain
Soil type	brown earth (66), regosol (131), rendzina (67), pseudogley (13)	Soil, pedological information
Soil development	developed (251), poorly developed (258), wet soil (26)	
USCS class	silty clay CL (58), organic silt OL (36), clayey silt CL-ML (128), silty sand SM (97), clayey gravel (26), silty to clayey gravel GC-GM (69), silty gravel GM (82)	
Macropores presence	few (367), many (108)	
Vegetation habitat	alternating mesic (104), alternating moist (44), mesic (79)	Vegetation
Meadow use intensity	intense (82), moderate (162)	
Meadow type	meadow (33), pasture (263)	
Forest mixture	>80% coniferous (157), >80% deciduous (36), mixed stand (109)	
Forest canopy cover	dispersed 20% (45), gappy 40% (62), loose 60% (74), normal 80% (81), dense 90% (39)	
Forest condition	damage area (60), old stand (83), damage area (12)	
Forest development stage	mainly 20-35 cm (31), mainly 35-50 cm (62), mainly >50 cm (51), diverse mixture (68), young growth (65), pole timber (25)	
Forest layering	single-layered (176), multi-layered (126), unstocked area (10)	
Slide plane interface	in soil (224), soil / bedrock (257), topsoil / soil (80), in bedrock (19)	Landslide Process
Flow or slide process	flow (172), slide (116)	
Landslide mechanism	rotation (144), translation (398)	
Intensity previous slides	clear signs (324), no clear signs (159)	Previous Landslides
Signs old slides	no (194), yes (536)	
Signs recent slides	no (683), yes (47)	
Amount of water flow	none (229), little (118), medium (110), much (118)	Hydrological information
Wetness of site	moist (594), wet (56), dry (11)	
Morphological class	horizontal concave (123), horizontal concave and vertical concave (22), horizontal concave and vertical convex (48), horizontal convex	Morphological information

https://doi.org/10.5194/egusphere-2026-2858
Preprint. Discussion started: 10 June 2026

	(70), horizontal convex and vertical convex (37), uniform (262), vertical convex (112)	
Geological interbedding	no (360), yes (370)	Geological information
Geologic soil unit	moraine (47), slope debris (455), slope loam (59)	

3.4 Susceptibility model training

Landslide susceptibility was modelled using the Random Forest algorithm (Cutler et al., 2012) in *R* (R-Core-Team, 2020). The Area Under the Curve (AUC) was used as performance metric. The AUC was derived from the receiver operating characteristic curves by successively varying the probability threshold in small increments. AUC values range from 0 to 1, where 1 indicates perfect discrimination and 0.5 corresponds to random prediction. As a widely used metric for susceptibility models, reported AUC values vary considerably among studies, typically ranging from about 0.7 to values close to 1 (Ado et al., 2022; Frattini et al., 2010). Although incorporating additional performance metrics, rather than relying solely on AUC, may provide a more robust evaluation of model quality, AUC offers a straightforward and comprehensive measure of a model's predictive performance across all possible probability thresholds (Reichenbach et al., 2018; Lobo et al., 2008).

Identical data preparation and training procedure was conducted for both the dependent and independent model. A raster grid with a spatial resolution of 10 m × 10 m was applied across the entire training and test study areas (Canton Bern and SLD study area perimeters), to which all explanatory variables were resampled. Variables with finer resolution were resampled to 10 m using bilinear interpolation, whereas variables with lower resolution were disaggregated to a 10 m resolution (without interpolation). Information derived from vector datasets was rasterized and assigned to the corresponding grid cells (10 m resolution). Following the recommendations of (Reichenbach et al., 2018), the spatial resolution was selected to best represent the landslide type under investigation. Analysis of the SLD inventory indicates a median landslide area of 135 m². Accordingly, a grid resolution of 10 m × 10 m (100 m² per cell) was selected. According to information from the swissTLM3D dataset (Swisstopo, 2025d), raster cells corresponding to buildings, lakes, glaciers, and rock outcrops were excluded from the analysis, under the assumption that shallow landslides do not occur in these areas.

For both the datasets (Canton Bern and SLD) a cell was classified as landslide-triggering if the centroid of a mapped landslide release area fell within it; all remaining cells were treated as non-triggering (Pourghasemi et al., 2020). To account for uncertainties in landslide delineation (Steger et al., 2016b) and to reduce potential spatial autocorrelation, different buffer zones were tested around landslide-triggering cells. However, no improvement in cross-validated model performance was observed (data not shown). Consequently, no buffer was applied in the analyses presented in this study.

Both models were trained based on the Canton Bern inventory. The independent model was validated and optimized using a spatial cross-validation scheme. The training area of the Canton Bern was partitioned into seven geographically distinct regions (Fig. 1; Hählen, 2024). In the seven-fold cross-validation, each region was used once as the test set, while the remaining six

https://doi.org/10.5194/egusphere-2026-2858
Preprint. Discussion started: 10 June 2026

regions served as the training set. AUC performance metrics were computed for each fold and arithmetic means over all fold were derived. Cross-validation was used to optimize the Random Forest hyperparameters employing a grid-search approach to evaluate the optimal combination of hyperparameters using all available explanatory variables (Liu et al., 2023). The optimum was achieved with 150 classification trees, and the number of variables randomly selected at each node (mtry) was set to the square root of the total number of explanatory variables. The minimum number of samples in each terminal node was set to five, and no maximum tree depth was imposed. Several strategies were tested to address the imbalance between non-triggering and triggering samples, including undersampling the majority class, oversampling the minority class, class weighting, and stratified sampling (Chen et al., 2004). Among these approaches, stratification with a factor of one yielded the best performance, whereas the remaining parameters were kept at their default settings. This means that each individual decision tree was trained on an equal number of triggering and non-triggering samples, randomly selected from all available samples. Following hyperparameter optimization, the optimal combination of explanatory variables for the independent model (i.e. the combination with the highest mean AUC of the cross validation) was identified by iteratively removing the least important variables based on permutation importance calculated on the cross-validation data.

The dependent model was validated and optimized based on the SLD dataset using identical hyperparameters as the independent model. Similarly to the independent model, the optimal combination of explanatory variables was identified by iteratively removing the least important variable based on permutation importance calculated over the SLD dataset. The combination yielding the highest AUC applied to the SLD perimeters was selected.

Ultimately, both models were separately trained with the optimal selection of explanatory variables based on the entire Canton Bern training area. Comparison of the two models revealed the influence of the selection of explanatory variables on transferability from the training to the distinct geographic regions of the SLD.

3.5 Application on the test inventory

Both the independently and the dependently trained models were applied to the test area to predict susceptibility of the SLD perimeter regions (Fig. 1). Model performance was evaluated using the AUC, computed both over the entire test area and separately for each perimeter. This allowed us to quantify the transferability of the Random Forest model to different perimeter regions from the SLD. To assess the influence of landslide inventory incompleteness on model performance, we evaluated whether the independent model produced different results when applied to the three SLD perimeters Napf_02, Napf_05, and Eriz_12 located within the canton of Bern (Fig. 1) using the more comprehensive Bern inventory instead of the SLD. While the SLD documents 159 landslides within these perimeters, the Bern inventory records 378 landslides, including most of those contained in the SLD.

To assess whether hidden variables explain limitations in the explanatory variables, we analysed whether variations in predicted susceptibility were systematically related to hidden variable classes. Systematic trends —for example, higher predicted susceptibility for more developed than for less developed soils— suggest that the hidden variable influences landslide

https://doi.org/10.5194/egusphere-2026-2858
Preprint. Discussion started: 10 June 2026

occurrence in a way not captured by the model. Specifically, landslides in classes associated with low predicted susceptibility may explain the occurrence of false negatives.

To quantify effects from individual hidden variables, we assigned each SLD landslide a susceptibility value from both models by calculating the area-weighted mean susceptibility across the estimated release area (Sect. 3.1.2), rather than using only the raster cell at the landslide centroid as in the performance analysis (Pourghasemi et al., 2020). Subsequently each landslide was ranked according to increasing susceptibility values. As rank-based statistics, we calculated eta-squared rank effect sizes (η^2):

$$\eta^2 = \frac{H - k + 1}{n - k}$$

where H is a rank-based group difference measure as computed based on the Kruskal-Wallis (1952) test, k is the number of categories per variable, and n is the total number of samples. Effect sizes range from 0 to 1 and quantify the degree to which an individual hidden variable (for example the USCS class) can explain the variance in modelled susceptibility. Effect sizes of 0.01 to 0.06 indicate small effects, 0.06 to 0.14 moderate effects, and larger than 0.14 large effects (Ben-Shachar et al., 2020). Boxplots display the susceptibility distribution for each individual category of the variables with the largest effect sizes, showing the interquartile range (Q1–Q3), the median, and whiskers extending to 1.5 times the interquartile range; values beyond this range are shown as outliers. Statistical differences between individual categories were competed by the Dunn's test with the conservative Bonferroni p-value adjustment method (Dunn, 1964). The analysis was performed for both the independent and dependent model. Hidden variables with consistently high effect sizes across both models provide evidence that trends are systemic, rather than being artifacts of a single model affected by limited spatial transferability.

4 Results

4.1 Performance of the Independent model

The optimized model resulted in a mean AUC of 0.89 across the seven cross-validation folds (Table 3), utilizing an optimal subset of 27 explanatory variables selected from the initial 33 (Table 1). Permutation-based feature importance (Fig. 2a) indicates that random shuffling of any retained variable would lead to a reduction in model performance. Slope gradient is by far the most influential predictor, causing an AUC decrease of 0.22 when permuted, followed by vegetation height and distance to the nearest stream. The average contribution of each explanatory variable is illustrated as partial dependence plots in Supplementary Material Fig. S1.

When the training data was re-substituted as test data into the final trained model, the model achieved an AUC of 0.93, indicating limited overfitting of the training dataset (compare to the cross-validation AUC of 0.89). Despite this, when the independent model was tested against the eight SLD perimeters, the overall average performance was considerably lower (AUC = 0.74) and varied strongly among perimeters. Susceptibility values likewise differ substantially between perimeters (Fig. 2b). AUC values across individual perimeters range from 0.66 for the *Sachseln_97* perimeter to 0.89 for the *Eriz_12* perimeter. The three perimeters located within the canton of Bern (*Eriz_12*, *Napf_02*, and *Napf_05*), which were excluded

https://doi.org/10.5194/egusphere-2026-2858
Preprint. Discussion started: 10 June 2026

from model training (Sect. 3.1.1), show comparatively higher average predicted susceptibility and AUC values up to 0.89, 0.75 and 0.76, respectively. An example of the high spatial variability in susceptibility prediction is shown for the perimeter *Sachseln_97* (Fig. 2c); maps of the other perimeters are provided in the Supplementary Material (Fig. S2)

To assess the effect of landslide inventory incompleteness of the SLD, the model was subsequently tested on the three perimeters located within the canton Bern, using the Bern inventory instead of the SLD. The results showed similar performance for the more complete Bern dataset, with AUC values of 0.88, 0.79, and 0.79, respectively.

Table 3. Comparison of area under the curve (AUC) performance for the different models and datasets.

	Independent model		**Dependent Model**	
	Area considered	AUC	Area considered	AUC
Training	Canton Bern	0.93	Canton Bern	0.92
Validation	Cross-Validation on Canton Bern	0.89	SLD perimeters	0.79
Test	SLD perimeters	0.74	SLD perimeters	0.79

https://doi.org/10.5194/egusphere-2026-2858
Preprint. Discussion started: 10 June 2026

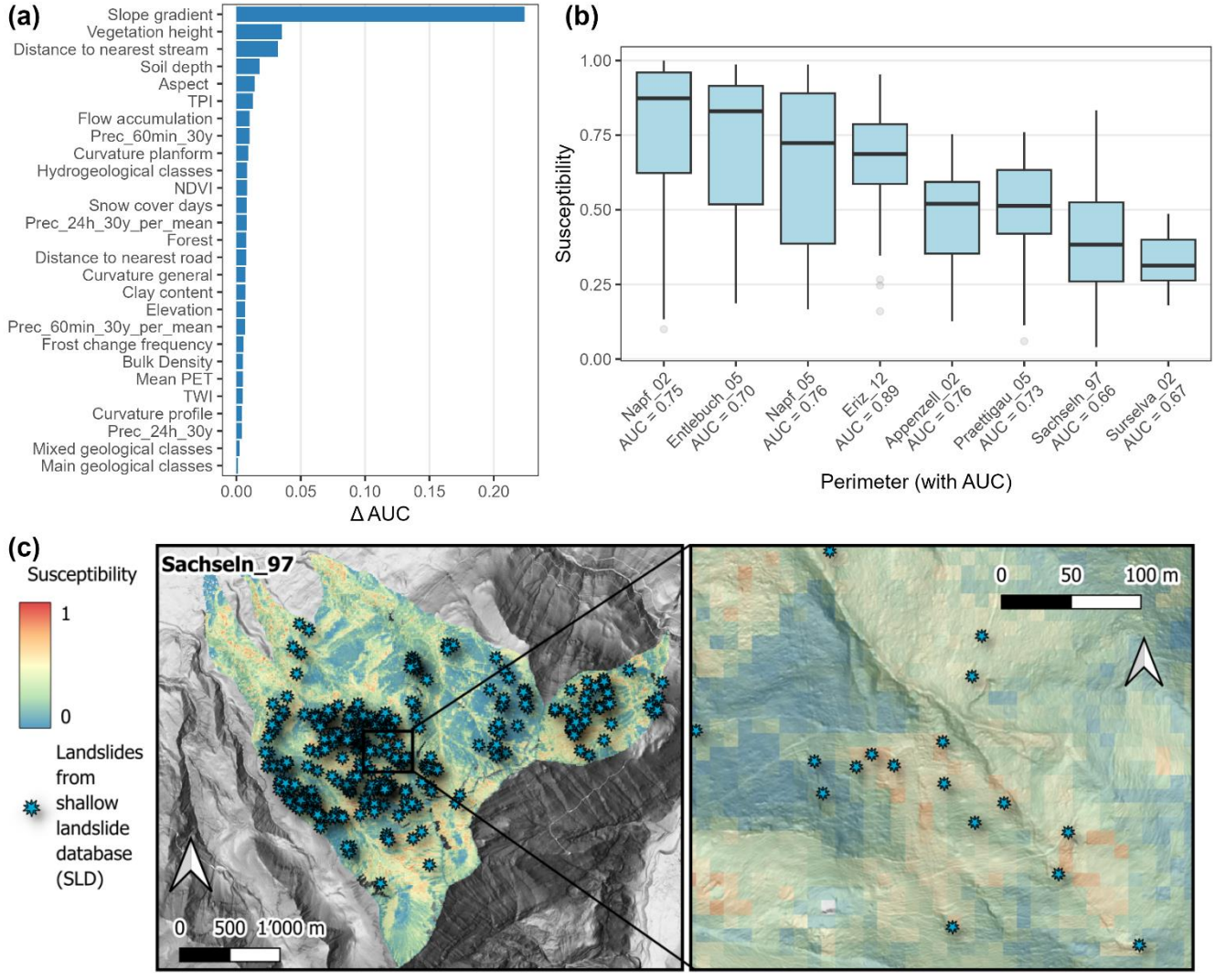

Fig. 2. Overview of the independent model. (a) Feature importance, expressed as the decrease in area under the curve (AUC) metric resulting from random permutation of each explanatory variable. (b) Comparison of predicted susceptibility distributions of the landslides in the shallow landslide database (SLD) across the test perimeters, including individual AUC performances. (c) Landslide susceptibility map of the test perimeter *Sachseln_97* (left) with a zoomed-in map to illustrate the high variability in susceptibility predicted by the model (right).

4.2 Comparison of the Independent and Dependent Model

The dependent model outperformed the independent model in the SLD test areas (AUC = 0.79 vs. 0.74, Table 3 and Fig. 3) as it can better represent small-scale susceptibility variation (compare Fig. 2c and Fig. 3c). Given the optimization on the test area, this improvement was expected; more informative however, was the comparison of the selected explanatory variables in the two models. Of the 33 available explanatory variables, the independent model relied on 27 variables to optimize performance in the Bern training area based on spatial cross-validation, whereas the dependent model selected only 19

https://doi.org/10.5194/egusphere-2026-2858
Preprint. Discussion started: 10 June 2026

variables to best represent the SLD test area (Table 1). None of the four categorical variables—*hydrogeological classes*, *geological classes* (*main and mixed*), and the binary *forest* attribute—used in the independent model were retained in the dependent model. In addition, *elevation*, *bulk density*, *distance to the nearest road*, and several climatic variables including *mean potential evapotranspiration (PET)*, *frost change frequency*, *mean precipitation*, and both *ratios between extreme and mean annual precipitation (Prec_60min_30y_per_mean and Prec_24h_30y_per_mean*) were excluded. Conversely, the three variables *silt content*, *growing season length*, and *mean annual temperature* were included only in the dependent model.

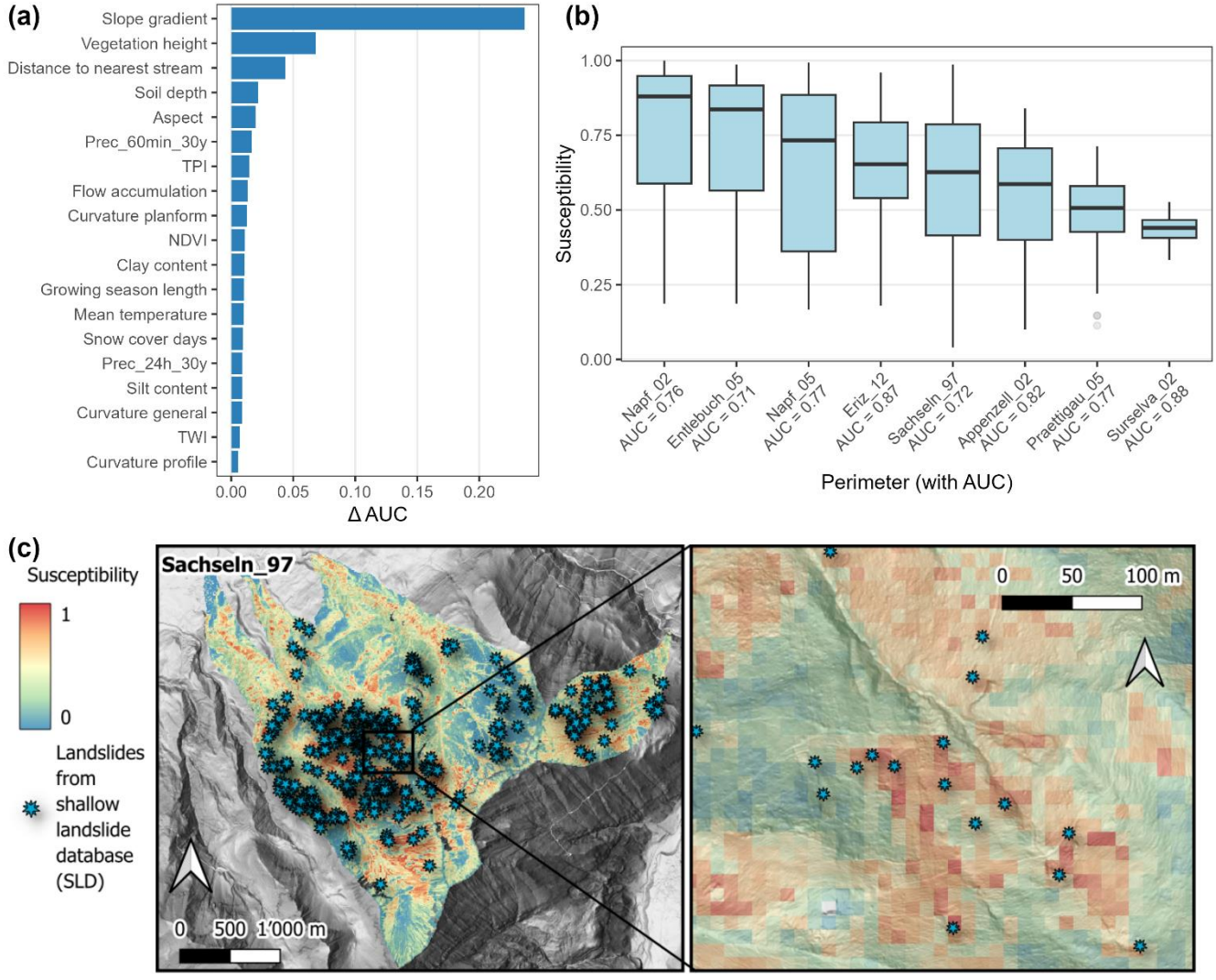

Fig. 3. Overview of the dependent model. (a) Feature importance, expressed as the decrease in area under the curve (AUC) metric resulting from random permutation of each explanatory variable. (b) Comparison of predicted susceptibility distributions of the landslides in the shallow landslide database (SLD) across the test perimeters, including individual AUC performances (c) Landslide susceptibility map of the test perimeter *Sachseln_97* (left) with a zoomed-in map to illustrate the high variability in susceptibility predicted by the model (right).

https://doi.org/10.5194/egusphere-2026-2858
Preprint. Discussion started: 10 June 2026

4.3 The Role of Hidden Variables in False Negatives

To assess whether hidden variables contribute to false negatives and systematically influence model transferability, effect sizes were computed using the Kruskal–Wallis test based on susceptibility predictions for the SLD dataset for both the dependent and independent models. Susceptibility predictions were compared with field information from the SLD and Fig. 4 summarizes the effect sizes of each hidden variable across both models. The effect sizes of the dependent model (Fig. 4a) were smaller than those of the independent model (Fig. 4b), which can be related to the higher performance of the dependent model, leading to smaller variation among susceptibility prediction of the SLD landslides. In both models, variables related to soil (pedological) and vegetation exhibited the highest effect sizes, with soil type, USCS class, soil development, slide plane interface, and forest layering consistently ranking among the six most influential variables.

The susceptibility distributions of the categories of these five variables are shown for the dependent model in Fig. 5 (and in the Supplementary Material Fig. S3 for the independent model) for all perimeters combined (top row) and for individual SLD perimeters (all other rows). The latter allow assessment of whether overall variability can be explained by susceptibility differences between perimeters. The analysis focuses on results from the dependent model, which is less affected by transferability issues than the independent model (Sect. 4.2). The differences between individual categories of the hidden variables were generally small due to the relatively low effect sizes of this model (maximally 0.06, Fig. 4a). Particular attention is given to categories associated with relatively low predicted susceptibility, as these may indicate conditions insufficiently captured by the model.

Landslides occurring in Rendzina and Regosol soils were predicted to have lower susceptibility than those triggered in Brown Earth soils (Fig. 5, first column). This pattern can largely be attributed to the Sachsln_97 perimeter, which contained most of the soil-type information. Landslides in poorly developed soils (such as Rendzina and Regosol) exhibited significantly lower predicted susceptibility ($p < 0.05$) compared to those in more developed soils (e.g., Brown Earth). This trend was consistent across individual perimeters with at least 10 landslides (Fig. 5, second column). Comparison between soil development and soil depth information from the SLD indicated significantly greater soil depths in developed (median depth ≈ 0.8 m) compared to poorly developed soils (median depth ≈ 0.5 m). Landslides in silty gravel (GM) and silty sand (SM) corresponded to the highest susceptibility (Fig. 5, third column), while the soil class organic silt (OL) was predicted with the lowest susceptibility (statistically significant: $p < 0.05$). Comparisons within individual perimeters show similar, yet insignificant, trends due to the comparably lower number of samples in each category. Overall, there is no systematic trend that coarser nor finer grained USCS-soil classes are better or worse predicted by the dependent model.

Significantly higher susceptibility ($p < 0.05$) was associated with slide planes at the interface between topsoil (humus or organic layer) and soil, compared to failures at the soil–bedrock interface or entirely within the soil material (Fig. 5, fourth column). This variation can largely be explained by susceptibility differences between the perimeters. Only the Napf_05 perimeter showed a significant trend with lower susceptibility predicted for failure within the soil layer, compared to failure at the interface between topsoil and soil. Predicted susceptibility was generally lower for landslides in single-layered forests than in

https://doi.org/10.5194/egusphere-2026-2858
Preprint. Discussion started: 10 June 2026

480 multi-layered forests (see Fig. 5, fifth column). However, no statistically significant differences were observed for any of the parameters.

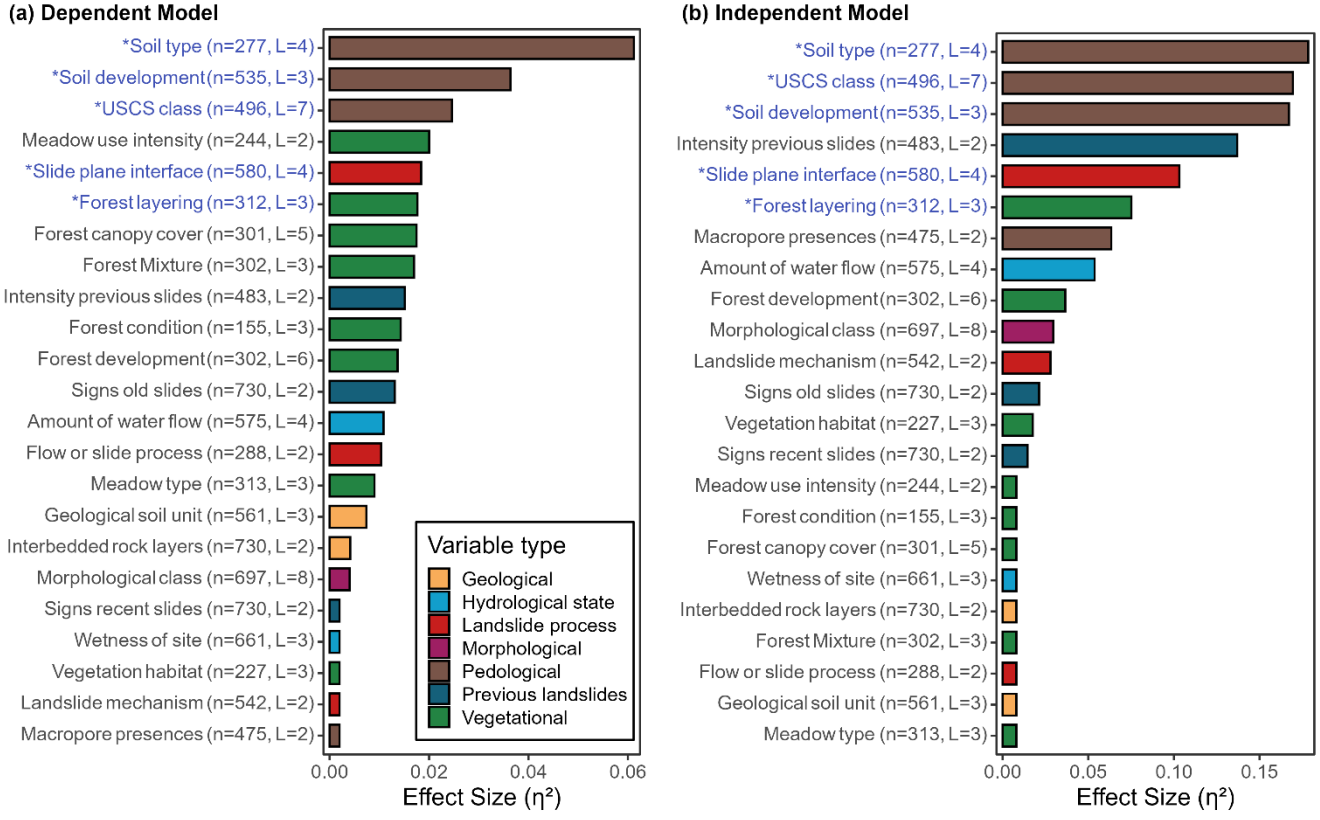

Fig. 4. Ranked effect sizes (η²) indicating the proportion of variance in predicted landslide susceptibility explained by individual
485 **hidden variables extracted from the shallow landslide database (SLD). For each variable, the number of samples (n) and the number of individual categories (L) are reported. Highest ranking variables of both models are marked with an asterisk (*) and susceptibility values of the individual categories are shown in Fig. 5.**

https://doi.org/10.5194/egusphere-2026-2858
Preprint. Discussion started: 10 June 2026

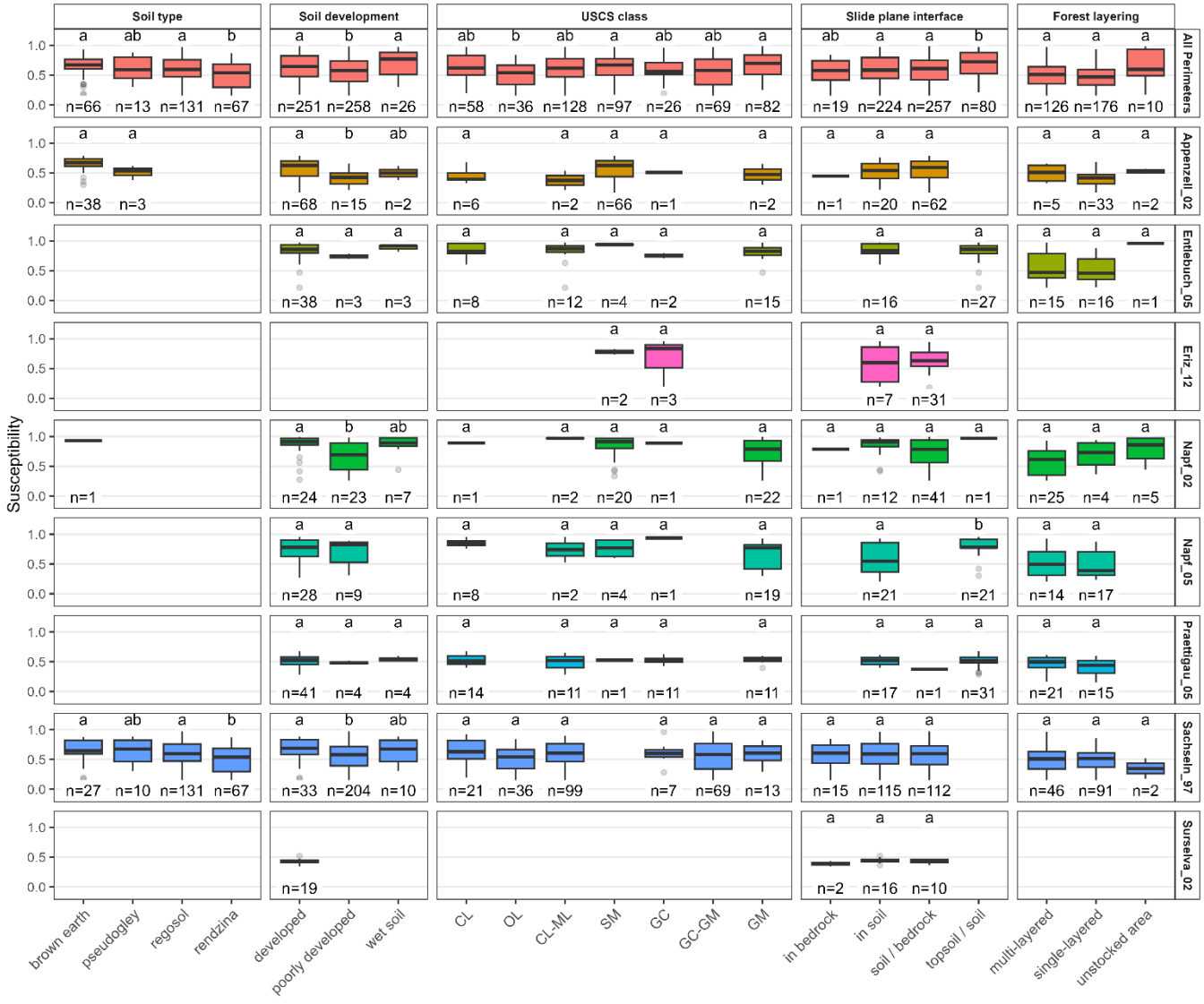

Fig. 5. Distribution of predicted susceptibility values based on the dependent model of the hidden variables with the highest effect sizes (Fig. 3), shown as compound overall perimeters (top row) and separately for each SLD perimeter (bottom rows). Lowercase letters denote statistical significance ($p < 0.05$) based on Dunn's test with Bonferroni p-value adjustments; distinct letters indicate significant differences between groups within the same category and perimeter. Unified Soil Classification System (USCS) are sorted from fine-grained to coarse-grained classes: CL = silty clay, OL = organic silt, CL-ML = clayey silt, SM = silty sand, GC = clayey gravel, GC-GM = silty to clayey gravel, GM = silty gravel.

https://doi.org/10.5194/egusphere-2026-2858
Preprint. Discussion started: 10 June 2026

5 Discussion

5.1 General Model performance and Study Limitations

The wide range of explanatory variables available for Switzerland from public repositories (Sect. 3.2) contribute to the relatively high performance of the independent model with a mean cross-validation AUC = 0.89 (compared to international studies e.g. Merghadi et al., 2020; Rossi et al., 2010). However, such comparisons must be made with caution as the performance strongly depends on the model design. As outlined in Sect. 2, several factors may influence performance, including the choice of algorithm (Pourghasemi and Rahmati, 2018; Goetz et al., 2015), mapping unit (Erener and Düzgün, 2012; Ma et al., 2023), spatial resolution (Karsa et al., 2019; Lee et al., 2004) and sampling strategy (Gu et al., 2024; Lai et al., 2019). While the effects of these choices on performance metrics are an important subject, practical considerations and the usability of resulting susceptibility maps must be taken into account (Goetz et al., 2015; Reichenbach et al., 2018).

To this end, we developed a susceptibility model approach to investigate limitations that are less commonly considered. Although other modelling approaches may achieve higher predictive performance, our aim was to highlight limitations that may apply not only to the selected method but more broadly to landslide susceptibility research. However, we note that these limitations are not independent of the chosen model design, which introduces uncertainty to the overall study framework. Additional sources of uncertainty are related to the use of AUC as the performance metric. While AUC enables straightforward evaluation independent of a susceptibility cut-off threshold, its absolute value must be interpreted with caution (Lobo et al., 2008). For example, including easily classifiable areas such as plains artificially inflate model performance (Steger et al., 2017). In addition, areas predicted with high susceptibility, but no observed landslides (false positives) do not necessarily indicate incorrect predictions. Instead, the observation period may have been too short for triggering conditions to occur (Huang et al., 2024; Zêzere et al., 2009). This is particularly relevant for highly localized rainfall events that trigger landslides only in limited parts of the landscape, as observed in the SLD inventories (Rickli, 2001). In such cases, AUC values may be relatively low even though predictions of localized high susceptibility are realistic. Furthermore, data-driven models trained in areas that have not yet experienced landslides—but may fail in the future—are also biased in learning true landslide causes.

5.2 Inventory Incompleteness Limitations

The training and validation inventory of the canton Bern includes more than 24,000 landslides across 5,939 km², providing a dense and comprehensive dataset for model development (Petschko et al., 2014). To study the influence of landslide inventory incompleteness, we applied the independent model on the two individual inventories considering identical perimeters areas (both datasets were excluded from model training). Applying the model to the Bern inventory (AUC = 0.88, 0.79, 0.79 for Eriz_12, Napf_05, and Napf_02) instead of the SLD (0.89, 0.76, 0.75) produced comparable results. Although the SLD inventory contains significantly fewer landslides (159 instead of 378) documented after single extreme rainfall event, landslide inventory incompleteness only had a minor influence on the lower performance of the test on the SLD (AUC = 0.74). The analysis, however, does not evaluate the degree of inventory incompleteness of the Bern training data and its overall effect on

https://doi.org/10.5194/egusphere-2026-2858
Preprint. Discussion started: 10 June 2026

model performance. Although the inventory combines both visually identifiable landslides from regularly updated high-resolution orthophotos as well as reported landslide from an official inventory (Sect. 3.1.1), the inventory cannot be considered complete. Incompleteness of landslide inventories is inherent to all databases (Steger et al., 2017; van Westen et al., 2008). With visually mapped landslides based on orthophoto having been shown to incompletely document landslide occurring in forest, because forest stands may cover the geomorphic features (Jacobs et al., 2017), while public reports may overrepresent landslides closer to infrastructure (Liechti et al., 2022; Steger et al., 2016a).

5.3 Transferability Limitations

The primary cause of reduced test performance of the test compared to the training (AUC = 0.74, compared to 0.89) is related to limited model transferability to distinct geographic regions with contrasting environmental conditions. Von Ruette et al. (2011) analysed model transferability using a subset of the SLD by training a logistic regression susceptibility model on the Napf_05 perimeter and applying it to the independent perimeters Napf_02 (AUC = 0.72), Entlebuch_05 (AUC = 0.69), and Appenzell_02 (AUC = 0.82). These performance values are comparable to those obtained in this study for the independent model using a Random Forest model trained on the Bern inventory (AUC = 0.75, 0.70, and 0.76, respectively). In the present study we further found that perimeters located within the training area (though excluded from training) exhibit substantially higher median predicted susceptibility and performance (mean AUC = 0.80) than perimeters outside the training region (mean AUC = 0.70; Fig. 2). Similarly, cross-validation performance is considerably higher (mean AUC = 0.89), due to the spatial proximity between training and validation folds and the use of a single inventory. These findings indicate that the model is not overfitted; rather, it is well calibrated for environments similar to the training region but struggles to generalize to areas with differing geographic, climatic, and geological conditions.

Comparing the independent (AUC = 0.74, trained on Bern, optimized to cross validation) to the dependent model (AUC = 0.79, trained on Bern, optimized for the SLD) revealed that the lower performance of the former model may reflect a non-optimal selection of explanatory variables. The optimized dependent model relied on 19 rather than 27 variables, excluding specifically all categorical predictors as well as many regional geology- and climate-related variables (Table 1), while most numerical variables relevant to describe small-scale variation were retained. These results suggest that incorporating regional (climatic and geologic) information does not necessarily improve prediction accuracy in independent areas. Instead, regional variables may reduce model transferability when the training and test regions are geographically distinct.

5.4 Influence of Non-Represented Environmental Variables

Even though mismatches can partly be explained by previously discussed limitations in transferability, they are evident in both the training and testing datasets and were often observed in close proximity to correctly predicted landslides.

Detailed analyses of hidden SLD variables indicated that these predictive gaps are likely linked to critical factors absent from large-scale spatial datasets. Variables attributed to soil and vegetation information yielded highest effect sizes (Fig. 4) with consistent —albeit partly weak—trends across perimeters (Fig. 5). These findings support the interpretation that subsurface

https://doi.org/10.5194/egusphere-2026-2858
Preprint. Discussion started: 10 June 2026

heterogeneity and vegetation structure act as locally relevant controls on slope stability, contributing to residual model errors that cannot be resolved at the current spatial scale, a point that warrants further discussion and explanation. The variations of the hidden variable slide plane interface could be attributed to susceptibility differences between individual perimeters (Fig. 5) and was therefore not further discussed.

5.4.1 Subsurface Heterogeneity

Landslides in poorly developed soils were predicted with significantly lower susceptibility than well-developed soils ($p < 0.05$, Fig. 5). Poorly developed soils were not only less well predicted by our model but are also slightly more common in our database compared to developed soils (258 vs. 251). Given that soil development is time-controlled (Duchaufour, 1982) and that the last glacial maximum dates back to the Würm glaciation (19,000 - 24,000 years), sufficient time would generally have been available for soil development in the study area (Hartmann and Blume, 2024). The frequent occurrence of landslides in poorly developed soils therefore warrants closer examination.

One potential controlling key effect of soil development is soil depth. Landslides in Rendzina soils, which are characterized by a shallow depth to bedrock, were predicted with significantly lower susceptibility than landslides in Regosol and Brown Earth (Fig. 5). Across all 509 landslides with available soil depth information, those occurring in developed soils initiated at statistically significantly greater depths (median ≈ 0.8 m) than those in poorly developed soils (≈ 0.5 m). Compared to deeper soils, shallow soils have lower water storage capacity and saturate more rapidly, accelerating suction loss and pore-water pressure buildup during rainfall (Godt et al., 2009; Callahan et al., 2020). This likely contributes to the higher failure probability of shallow soils (Peres and Cancelliere, 2016). While the DEM-based soil depth proxy used as an explanatory variable (sGIST; Catani et al., 2010, Sect. 3.2.5) indicated a similar trend with a lower median soil depth index in poorly developed compared to developed soils (median ≈ 0.06 and 0.08 respectively; Fig. S4), this variable did not sufficiently capture the local complexity relevant to failure processes.

Furthermore, finer-grained soils (higher silt and clay content) can be related to reduced shear strength, as soils tend to be better mechanically supported by larger grains compared to soils with predominantly fine grains (Vallejo, 2011) and since the reduction in soil suction during infiltration is stronger in fine-grained soil (Lu et al., 2010). Although no systematic trend was observed across the different USCS soil classes, landslides occurring in the fine-grained class organic silt (OL) were least well represented by the model. In contrast, landslides in the coarse-grained classes silty sand (SM) and silty gravel (GM) were best predicted by the dependent model with significantly highest susceptibility (Fig. 5).

Beyond texture, soil structure—particularly macropore networks—plays a critical role in subsurface hydrology. Preferential flow paths are typically better developed in older soils, promoting efficient lateral drainage, whereas younger soils tend to exhibit predominantly vertical flow (Hartmann and Blume, 2024). Accordingly, only 13 landslides with many macropores were found in poorly developed soils in the SLD, compared to 92 in developed soils. While higher permeability can enhance drainage and stability, strong contrasts can promote slope failure during intense rainfall. For example, if highly permeable

https://doi.org/10.5194/egusphere-2026-2858
Preprint. Discussion started: 10 June 2026

layers are superimposed by layers with low permeability, or when highly permeable layers narrow downhill, sudden increases in pore-pressure accumulation may occur (Rickli, 2001).

Finally, soil development is closely linked to bedrock weathering (Blume et al., 2016). Bedrock beneath poorly developed soils is likely less weathered due to reduced time exposure, forming sharp hydrological and mechanical contrasts at the soil–bedrock interface. Such interfaces can concentrate subsurface flow and promote pore-pressure buildup and low-shear-strength horizons. The stability of these interfaces is strongly lithology dependent. Advanced weathering does not necessarily indicate stabilization. For instance, heavily weathered marl bedrock can form fine-grained layers with unfavourable geotechnical properties, as observed in the Sachseln perimeter (Rickli, 2001).

Although local bedrock properties are known to strongly influence slope stability (Roda-Boluda et al., 2018; Selby, 1982; Moon et al., 2026) this study considered only broad geological units. Information which only differs regionally such as lithological variations, could not be represented in large-scale susceptibility models, due to their inherent limitation of summarisation trends over larger areas. On the other hand, the explanatory variables included in the model cannot capture actual small-scale subsurface heterogeneity. While the factors discussed here illustrate some of this complexity, many additional controls on slope stability, such as the effect of spatial and temporal heterogeneity of soil wetness (Ray et al., 2011) or soil aggregate stability (Bast et al., 2015; 2016) , remain unresolved by the field information available in the SLD.

5.4.2 Vegetation Complexity

Vegetation exerts a strong control on shallow landslide susceptibility, and the explanatory variables vegetation height and NDVI used in this study could not capture the full complexity of vegetation effects on slope stability. In both the dependent and the independent model, forest layering was among the hidden variable exhibiting highest effect size (Fig. 4). Landslides occurring in multi-layered forest were better represented by the susceptibility model by predicting slightly higher susceptibility than for landslides occurring in single-layered forests. However, it must be noted that the differences between multi-layered and single-layered forest is only statistically significant in the independent model (Fig. S3), but not in the dependent model (Fig. 5).

Single-layered forests are often composed of monospecific stands of similar age, which tend to exhibit more uniform root distributions (Ma and Chen, 2017). Mechanical reinforcement in such systems is concentrated within a limited soil depth where root density is highest. Interfaces between these uniformly rooted layers and root-free soil horizons may represent zones of reduced shear strength and increased instability. Additionally, single-layered forests typically exhibit lower canopy interception due to a comparatively smaller leaf area index (Bequet et al., 2012), resulting in increased peak infiltration during rainfall events. At the same time, reduced evapotranspiration rates of single-layered forests (Večeřa et al., 2019) can lead to higher antecedent soil moisture conditions prior to rainfall events, which induce prior stress on slope stability (Wicki et al., 2020; Halter et al., 2025a and 2025b).

In contrast, multi-layered and loose forests are characterized by a diverse vertical structure with a wide range of tree heights (Bast et al., 2025), which in turn results in a broader distribution of root diameters and rooting depths (Schmidt et al., 2001).

https://doi.org/10.5194/egusphere-2026-2858
Preprint. Discussion started: 10 June 2026

This structural diversity promotes a mechanically reinforcing root network that spans through the soil profile, with water percolating and draining efficiently along root channels. Understory and ground vegetation further contribute to slope stability by protecting the soil surface from erosion and enhancing soil aggregate stability (Zhang et al., 2018; Miyata et al., 2009).

It should be noted that forest layering and canopy cover represent only limited aspects of vegetation complexity. Beyond these attributes, vegetation influences landslide susceptibility through multiple mechanisms that were not captured by the explanatory variables used in this study nor by any hidden variable contained in the SLD. For example, studies have shown that local slope stability strongly depends on plant species, due to differences in mechanical root reinforcement (Bischetti et al., 2009; Schmidt et al., 2001) and canopy interception (Deguchi et al., 2006). Tree density further modulates the stabilizing effect of vegetation, with larger tree gaps generally associated with reduced slope stability (Bast et al., 2026; Moos et al., 2016).

5.5 Dynamic Slope Interactions and Implications for Landslide Susceptibility Modelling

The importance of vegetation and subsurface development further highlights the crucial role of time in understanding continuously evolving landscapes. In this study, explanatory variables were treated as static, representing conditions at a single point in time (van Westen et al., 2008). As a result, these variables may not adequately reflect the specific environmental conditions at the moment of landslide occurrence. Incorporating time-updated explanatory variables could help address this limitation by capturing the dynamic nature of subsurface conditions, vegetation, and landscape morphology, which evolve in response to both natural processes and human activities (Jones et al., 2021).

Furthermore, the processes and factors that form and shape the environment, and thereby influence slope stability, are dependent on each other. In the context of this discussion, soil development is fundamentally coupled with vegetation dynamics, as biological activity enhances both chemical and physical weathering rates (Blume et al., 2016). Fully developed soils can occur only in conjunction with advanced stages of vegetation succession; conversely, vegetation succession is inherently linked to the degree of soil development (Duchaufour, 1982). Landslide susceptibility must be understood within the framework of a dynamic earth system which constantly evolves and in which interacting processes influence one another (Sidle and Bogaard, 2016).

In complex natural systems, landslide failure may be controlled by different dominant factors at different locations, or by the interaction of multiple factors. Insight into hidden variables enable a unique opportunity to study these factors, however they cannot unravel the many multi-dimensional complexity relevant to slope stability. Although advanced machine-learning models attempt to capture dependencies among explanatory variables, they cannot yet represent the full complexity of natural systems, underscoring the continued need for process-based understanding. While physically based models explicitly aim to reproduce this complexity, their application at large spatial scales and high resolution remains computationally constrained. Moreover, they may be even more sensitive to incomplete surface and subsurface information than data-driven approaches (Godt et al., 2008). This highlights the importance of acquiring detailed and timely-updated high-quality environmental data.

https://doi.org/10.5194/egusphere-2026-2858
Preprint. Discussion started: 10 June 2026

Comprehensive in-situ measurements and advanced remote-sensing technologies represent promising steps towards reducing these limitations.

6 Conclusion

Based on literature review, four major limitations of data-driven landslide susceptibility models were identified. Three of these limitations (b-d) were studied through a case study framework based on two independent landslide inventories and two model approaches trained with Random Forest:

a. Model design limitations relate to non-optimal modelling choices, such as the selection of the model algorithm, mapping units, spatial resolution, and sampling strategy. As many studies have examined these aspects in detail, we relied on established best practices to develop a robust study design. Beyond predictive performance, the reliability and practical usability of the resulting susceptibility maps must be considered.

b. The influence of inventory completeness limitations was assessed by comparing model performances using two inventories with different levels of detail. The results indicated that incompleteness of the SLD test dataset only slightly reduced prediction accuracy. However, the potential impact of incompleteness in the training inventory remained unresolved, and positional inaccuracies may introduce biases during model training.

c. Applying the trained susceptibility models to geographically distinct test regions revealed major limitations in transferability. While the models achieved high predictive performance within the training area (mean cross-validation AUC = 0.89), performance decreased substantially when applied to independent test areas (AUC = 0.74 for the independent model and 0.79 for the dependent model), with uncertainty increasing with distance from the training domain. Comparison between the independent model (trained and optimized on the training area) and the dependent model (optimized for the test area) further showed that the selection of explanatory variables strongly affects transferability. Regional climatic and geological variables that improved performance within the training area reduced model generalization to remote regions.

d. Hidden variables from 734 landslides documented in field investigation revealed that the subsurface heterogeneity and vegetation complexity could not sufficiently be represented by the explanatory variables. Specifically, landslide susceptibility was underestimated in poorly developed and in single-layered forests. Advanced soil development may enhance slope stability through greater soil depth, increased water storage capacity, and delayed pore-pressure buildup. In addition, well-developed soil structures with abundant macropores likely promote efficient subsurface drainage. Single-layered forests exhibit more uniform root distributions, lower canopy interception, and reduced evapotranspiration. These factors lead to weaker mechanical root reinforcement, increased water infiltration, and higher antecedent soil moisture, all of which can reduce slope stability.

https://doi.org/10.5194/egusphere-2026-2858
Preprint. Discussion started: 10 June 2026

We conclude that, although research in the field of landslide susceptibility has greatly improved the quality and reliability of model predictions, uncertainties remain. Particularly we emphasize the need for detailed and complete landslide inventories for accurate modelling as well as high-resolution spatial datasets to better represent the complexity of surface and subsurface conditions controlling slope stability. Advances in remote sensing will be crucial for both data-driven and physically based approaches, as both depend on accurate characterization of above- and below-ground conditions at fine spatial resolution. To advance landslide research, this study underscores the continued need for process-based investigations grounded in field observations.

Supplement link

The supplementary material is published as separate file with this article.

Code and data availability

The code used for data processing, analysis, and visualization was developed in *R* (R-Core-Team, 2020) and QGIS (Dawson et al., 2025) and is available upon request from Tobias Halter (tobias.halter@wsl.ch). Datasets used in this study cannot be uploaded to a public database, due to individual data policies depending on the provider. Data from the shallow landslide database (SLD) are available through the repository of Rickli et al., (2016)**.** The national high-resolution digital elevation model *swissALTI3D* (Swisstopo, 2025a) and the topographic landscape model *swissTLM3D* (Swisstopo. 2025d) are provided by Swisstopo. The Swiss vegetation height model is available from Ginzler (2023), and the Normalized Difference Vegetation Index (NDVI) from UniGeneva, (2019). Geological data can be obtained upon request from Swisstopo (2025b). Climate data from CHELSA are publicly available at global scale (Karger et al., 2017). Extreme precipitation data (Fukutome et al., 2023) are available for Switzerland upon request from Sophie Fukutome (sophie.fukutome@meteoswiss.ch). Soil texture Swiss maps from the Soil Competence Center (KOBO, 2024) are available upon request to service@ccsols.ch. Mean precipitation and temperature data from Daymet (MeteoSwiss, 2024) are available for the scale of Switzerland upon request from Luzi Bernhard luzi.bernhard@wsl.ch. Bulk density data are available globally through SoilGrids (Poggio et al., 2021).

Author contributions

MS, JA and TH initiated and conceptualised the study. TH collected, processed, and analysed the data. TH performed the visualization and wrote the original draft of the manuscript. PL, AB, JA, and MS supervised the work. All authors reviewed and edited the manuscript.

Competing interests

The authors declare no competing interests nor financial interests.

https://doi.org/10.5194/egusphere-2026-2858
Preprint. Discussion started: 10 June 2026

Acknowledgements

We thank all individual providers of spatial data (Section: Code and data availability). Specifically, we thank Christian Rickli for providing data and insight into the shallow landslide database (SLD). Further, we thank Simone Grätzer for computing the soil depth map at national scale using the sGIST approach (Catani et al., 2010), and Lorenz Walthert for discussing effects of soil development on slope hydrology and stability.

References

Ado, M., Amitab, K., Maji, A. K., Jasińska, E., Gono, R., Leonowicz, Z., and Jasiński, M.: Landslide susceptibility mapping using machine learning: a literature survey, Remote Sens., 14, 3029, https://doi.org/10.3390/rs14133029, 2022.

Akinci, H. and Zeybek, M.: Comparing classical statistic and machine learning models in landslide susceptibility mapping in Ardanuc (Artvin), Turkey, Nat. Hazards, 108, 1515–1543, https://doi.org/10.1007/s11069-021-04743-4, 2021.

Ba, Q., Chen, Y., Deng, S., Yang, J., and Li, H.: A comparison of slope units and grid cells as mapping units for landslide susceptibility assessment, Earth Sci. Inform., 11, 373–388, https://doi.org/10.1007/s12145-018-0335-9, 2018.

Bast, A., Wilcke, W., Graf, F., Lüscher, P., and Gärtner, H.: A simplified and rapid technique to determine an aggregate stability coefficient in coarse grained soils, CATENA, 127, 170–176, https://doi.org/10.1016/j.catena.2014.11.017, 2015.

Bast, A., Wilcke, W., Graf, F., Lüscher, P., and Gärtner, H.: Does mycorrhizal inoculation improve plant survival, aggregate stability, and fine root development on a coarse-grained soil in an alpine eco-engineering field experiment?, J. Geophys. Res. Biogeosciences, 121, 2158–2171, https://doi.org/10.1002/2016JG003422, 2016.

Bast, A., Hobi, M. L., Ginzler, C., Piermattei, L., Fischer, C., Nikolova, P. S., Bührle, L. J., Kalt, T., and Graf, F.: An approach to detect and map forest canopy layers in Swiss mountain forests using nationwide airborne laser scanning data, Int. J. Appl. Earth Obs. Geoinformation, 145, 104986, https://doi.org/10.1016/j.jag.2025.104986, 2025.

Bast, A., Graf, F., Nikolova, P. S., Piermattei, L., Rickli, C., Hobi, M. L., and Ginzler, C.: Deriving and assessing forest gap thresholds to prevent shallow landslides in Swiss mountain forests, For. Ecol. Manag., 608, 123589, https://doi.org/10.1016/j.foreco.2026.123589, 2026.

Baum, R. L. and Godt, J. W.: Early warning of rainfall-induced shallow landslides and debris flows in the USA, Landslides, 7, 259–272, https://doi.org/10.1007/s10346-009-0177-0, 2010.

Ben-Shachar, M. S., Lüdecke, D., and Makowski, D.: Effectsize: estimation of effect size indices and standardized parameters, J. Open Source Softw., 5, 2815, https://doi.org/10.21105/joss.02815, 2020.

Bequet, R., Campioli, M., Kint, V., Muys, B., Bogaert, J., and Ceulemans, R.: Spatial variability of leaf area index in homogeneous forests relates to local variation in tree characteristics, For. Sci., 58, 633–640, https://doi.org/10.5849/forsci.10-123, 2012.

Beven, K. and Germann, P.: Macropores and water flow in soils, Water Resour. Res., 18, 1311–1325, https://doi.org/10.1029/WR018i005p01311, 1982.

https://doi.org/10.5194/egusphere-2026-2858
Preprint. Discussion started: 10 June 2026

Bischetti, G. B., Chiaradia, E. A., Epis, T., and Morlotti, E.: Root cohesion of forest species in the Italian Alps, Plant Soil, 324, 71–89, https://doi.org/10.1007/s11104-009-9941-0, 2009.

Blume, H.-P., Brümmer, G. W., Fleige, H., Horn, R., Kandeler, E., Kögel-Knabner, I., Kretzschmar, R., Stahr, K., and Wilke, B.-M.: Scheffer/SchachtschabelSoil Science, Springer Berlin Heidelberg, Berlin, Heidelberg, ISBN: 978-3-642-30941-0, https://doi.org/10.1007/978-3-642-30942-7, 2016.

Brönnimann, C., Stähli, M., Schneider, P., Seward, L., and Springman, S. M.: Bedrock exfiltration as a triggering mechanism for shallow landslides, Water Resour. Res., 49, 5155–5167, https://doi.org/10.1002/wrcr.20386, 2013.

Budhu, M.: Soil Mechanics Fundamentals, John Wiley & Sons, 370 pp., ISBN: 978-1-118-89771-3, 2015.

Burton, A. and Bathurst, J. C.: Physically based modelling of shallow landslide sediment yield at a catchment scale, Environ. Geol., 35, 89–99, https://doi.org/10.1007/s002540050296, 1998.

Callahan, R. P., Riebe, C. S., Pasquet, S., Ferrier, K. L., Grana, D., Sklar, L. S., Taylor, N. J., Flinchum, B. A., Hayes, J. L., Carr, B. J., Hartsough, P. C., O'Geen, A. T., and Holbrook, W. S.: Subsurface weathering revealed in hillslope-integrated porosity distributions, Geophys. Res. Lett., 47, e2020GL088322, https://doi.org/10.1029/2020GL088322, 2020.

Catani, F., Segoni, S., and Falorni, G.: An empirical geomorphology-based approach to the spatial prediction of soil thickness at catchment scale, Water Resour. Res., 46, W05508, https://doi.org/10.1029/2008WR007450, 2010.

Chen, C., Liaw, A., and Breiman, L.: Using random forest to learn imbalanced data, Univ. Calif. Berkeley, 110, 24, 2004.

Chicas, S. D., Li, H., Mizoue, N., Ota, T., Du, Y., and Somogyvári, M.: Landslide susceptibility mapping core-base factors and models' performance variability: a systematic review, Nat. Hazards, 120, 12573–12593, https://doi.org/10.1007/s11069-024-06697-9, 2024.

Chung, C.-J. F. and Fabbri, A. G.: Validation of spatial prediction models for landslide hazard mapping, Nat. Hazards, 30, 451–472, https://doi.org/10.1023/B:NHAZ.0000007172.62651.2b, 2003.

Clarke, B. A. and Burbank, D. W.: Quantifying bedrock-fracture patterns within the shallow subsurface: Implications for rock mass strength, bedrock landslides, and erodibility, J. Geophys. Res. Earth Surf., 116, https://doi.org/10.1029/2011JF001987, 2011.

Conrad, O., Bechtel, B., Bock, M., Dietrich, H., Fischer, E., Gerlitz, L., Wehberg, J., Wichmann, V., and Böhner, J.: System for Automated Geoscientific Analyses (SAGA) v. 2.1.4, Geosci. Model Dev., 8, 1991–2007, https://doi.org/10.5194/gmd-8-1991-2015, 2015.

Corominas, J., van Westen, C., Frattini, P., Cascini, L., Malet, J.-P., Fotopoulou, S., Catani, F., Van Den Eeckhaut, M., Mavrouli, O., Agliardi, F., Pitilakis, K., Winter, M. G., Pastor, M., Ferlisi, S., Tofani, V., Hervás, J., and Smith, J. T.: Recommendations for the quantitative analysis of landslide risk, Bull. Eng. Geol. Environ., 73, 209–263, https://doi.org/10.1007/s10064-013-0538-8, 2014.

Cutler, A., Cutler, D. R., and Stevens, J. R.: Random Forests, in: Ensemble Machine Learning: Methods and Applications, edited by: Zhang, C. and Ma, Y., Springer, New York, NY, 157–175, https://doi.org/10.1007/978-1-4419-9326-7_5, 2012.

Dahigamuwa, T., Yu, Q., and Gunaratne, M.: Feasibility study of land cover classification based on normalized difference vegetation index for landslide risk assessment, Geosciences, 6, 45, https://doi.org/10.3390/geosciences6040045, 2016.

https://doi.org/10.5194/egusphere-2026-2858
Preprint. Discussion started: 10 June 2026

Dawson, N., Fischer, J., Kuhn, M., Pasotti, A., Rouzaud, D., Bruy, A., Sutton, T., Dobias, M., Pellerin, M., Rouault, E., Olaya, V., Blottiere, P., Macho, W., Blazek, R., Sherman, G., Sant-anna, H., Cabieces, J., Bartoletti, L., Woodrow, N., Signedav, Rldhont, Shaffer, L., Natsis, S., Belgacem, N., Santilli, S., Larosa, S., Mani, S., Cloarec, V., and Jurgiel, B.: QGIS, , https://doi.org/10.5281/zenodo.17106590, 2025.

Defries, R. S. and Townshend, J. R. G.: Global land cover characterization from satellite data: from research to operational implementation?, Glob. Ecol. Biogeogr., 8, 367–379, https://doi.org/10.1046/j.1365-2699.1999.00139.x, 1999.

Deguchi, A., Hattori, S., and Park, H.-T.: The influence of seasonal changes in canopy structure on interception loss: Application of the revised Gash model, J. Hydrol., 318, 80–102, https://doi.org/10.1016/j.jhydrol.2005.06.005, 2006.

Duchaufour, P.: General principles of the origin and development of soils, in: Pedology: Pedogenesis and classification, edited by: Duchaufour, P., Springer Netherlands, Dordrecht, 108–156, https://doi.org/10.1007/978-94-011-6003-2_5, 1982.

Dunn, O. J.: Multiple Comparisons Using Rank Sums, Technometrics, 6, 241–252, https://doi.org/10.1080/00401706.1964.10490181, 1964.

Edrich, A.-K., Yildiz, A., Roscher, R., and Kowalski, J.: A modular framework for FAIR shallow landslide susceptibility mapping based on machine learning, https://doi.org/10.21203/rs.3.rs-3254996/v1, 2023.

Egli, M., Mirabella, A., and Sartori, G.: The role of climate and vegetation in weathering and clay mineral formation in late Quaternary soils of the Swiss and Italian Alps, Geomorphology, 102, 307–324, https://doi.org/10.1016/j.geomorph.2008.04.001, 2008.

Erener, A. and Düzgün, H. S. B.: Landslide susceptibility assessment: what are the effects of mapping unit and mapping method?, Environ. Earth Sci., 66, 859–877, https://doi.org/10.1007/s12665-011-1297-0, 2012.

Ermini, L., Catani, F., and Casagli, N.: Artificial Neural Networks applied to landslide susceptibility assessment, Geomorphology, 66, 327–343, https://doi.org/10.1016/j.geomorph.2004.09.025, 2005.

Fan, L., Lehmann, P., and Or, D.: Effects of soil spatial variability at the hillslope and catchment scales on characteristics of rainfall-induced landslides, Water Resour. Res., 52, 1781–1799, https://doi.org/10.1002/2015WR017758, 2016.

Fell, R., Corominas, J., Bonnard, C., Cascini, L., Leroi, E., and Savage, W. Z.: Guidelines for landslide susceptibility, hazard and risk zoning for land use planning, Eng. Geol., 102, 85–98, https://doi.org/10.1016/j.enggeo.2008.03.022, 2008.

Fischer, C. and Traub, B. (Eds.): Swiss national forest inventory – methods and models of the fourth assessment, Springer International Publishing, Cham, ISBN: 978-3-030-19292-1, https://doi.org/10.1007/978-3-030-19293-8, 2019.

Franklin, J.: Predictive vegetation mapping: geographic modelling of biospatial patterns in relation to environmental gradients - Janet Franklin, 1995, Prog. Phys. Geogr., 19, 474–499, https://doi.org/10.1177/030913339501900403, 1995.

Frattini, P., Crosta, G., and Carrara, A.: Techniques for evaluating the performance of landslide susceptibility models, Eng. Geol., 111, 62–72, https://doi.org/10.1016/j.enggeo.2009.12.004, 2010.

Fredlund, D. G. and Rahardjo, H.: Soil mechanics for unsaturated soils, John Wiley & Sons, ISBN: 978-0-470-17275-9, 1993.

Fukutome, S., Alouini, S., and Frei, C.: HYDROmaps - Extreme point precipitation, https://hydromaps.ch/#de/13/47.2753/9.3337/bl_hds--b04_extremprecip_60m_100a$33, 2023.

https://doi.org/10.5194/egusphere-2026-2858
Preprint. Discussion started: 10 June 2026

Fusco, F., Mirus, B. B., Baum, R. L., Calcaterra, D., and De Vita, P.: Incorporating the effects of complex soil layering and thickness local variability into distributed landslide susceptibility assessments, Water, 13, 713, https://doi.org/10.3390/w13050713, 2021.

Gabet, E. J. and Mudd, S. M.: The mobilization of debris flows from shallow landslides, Geomorphology, 74, 207–218, https://doi.org/10.1016/j.geomorph.2005.08.013, 2006.

GDAL/OGR contributors: GDAL/OGR geospatial data abstraction software library, Open Source Geospatial Found., https://doi.org/10.5281/zenodo.5884351, 2025.

Ghestem, M., Sidle, R. C., and Stokes, A.: The Influence of Plant Root Systems on Subsurface Flow: Implications for Slope Stability, BioScience, 61, 869–879, https://doi.org/10.1525/bio.2011.61.11.6, 2011.

Ginzler, C.: Vegetation height model national forest inventory (NFI), https://doi.org/10.16904/1000001.1, 2023.

Ginzler, C., Price, B., Bösch, R., Fischer, C., Hobi, M. L., Psomas, A., Rehush, N., Wang, Z., and Waser, L. T.: Area-Wide Products, in: Swiss National Forest Inventory – Methods and Models of the Fourth Assessment, edited by: Fischer, C. and Traub, B., Springer International Publishing, Cham, 125–142, https://doi.org/10.1007/978-3-030-19293-8_7, 2019.

Godt, J. W., Baum, R. L., Savage, W. Z., Salciarini, D., Schulz, W. H., and Harp, E. L.: Transient deterministic shallow landslide modeling: requirements for susceptibility and hazard assessments in a GIS framework, Eng. Geol., 102, 214–226, https://doi.org/10.1016/j.enggeo.2008.03.019, 2008.

Godt, J. W., Baum, R. L., and Lu, N.: Landsliding in partially saturated materials, Geophys. Res. Lett., 36, https://doi.org/10.1029/2008GL035996, 2009.

Goetz, J. N., Brenning, A., Petschko, H., and Leopold, P.: Evaluating machine learning and statistical prediction techniques for landslide susceptibility modeling, Comput. Geosci., 81, 1–11, https://doi.org/10.1016/j.cageo.2015.04.007, 2015.

Graf, F., Bebi, P., Braschler, U., De Cesare, G., Frei, M., Greminger, P., Grunder, K., Hählen, N., Rickli, C., Rixen, C., Sandri, A., Springman, S. M., Thormann, J.-J., von Albertini, N., and Yildiz, A.: Pflanzenwirkungen zum Schutz vor flachgründigen Rutschungen, WSL Berichte, Eidgenössische Forschungsanstalt für Wald, Schnee und Landschaft WSL, 2017.

GRASS Development Team: Geographic Resources Analysis Support System (GRASS) Software, Version 8.4, , https://doi.org/10.5281/zenodo.13102854, 2024.

Gu, T., Duan, P., Wang, M., Li, J., and Zhang, Y.: Effects of non-landslide sampling strategies on machine learning models in landslide susceptibility mapping, Sci. Rep., 14, 7201, https://doi.org/10.1038/s41598-024-57964-5, 2024.

Guadagno, F. M., Forte, R., Revellino, P., Fiorillo, F., and Focareta, M.: Some aspects of the initiation of debris avalanches in the Campania Region: the role of morphological slope discontinuities and the development of failure, Geomorphology, 66, 237–254, https://doi.org/10.1016/j.geomorph.2004.09.024, 2005.

Gutiérrez-Jurado, H. A. and Vivoni, E. R.: Ecogeomorphic expressions of an aspect-controlled semiarid basin: II. Topographic and vegetation controls on solar irradiance, Ecohydrology, 6, 24–37, https://doi.org/10.1002/eco.1263, 2013.

Guzzetti, F.: Landslide Hazard and Risk Assessment, Thesis, Universitäts- und Landesbibliothek Bonn, 2006.

Hählen, N.: Orthofotobasiertes Inventar spontaner, flachgründiger Rutschungen im Kanton Bern, 2024.

https://doi.org/10.5194/egusphere-2026-2858
Preprint. Discussion started: 10 June 2026

Halter, T., Lehmann, P., Bast, A., Aaron, J., and Stähli, M.: In situ soil moisture data improve precipitation-based shallow landslide early warning through innovative machine learning methods, Landslides, 22, 3599–3614, https://doi.org/10.1007/s10346-025-02599-4, 2025a.

Halter, T., Lehmann, P., Wicki, A., Aaron, J., and Stähli, M.: Optimising landslide initiation modelling with high-resolution saturation prediction based on soil moisture monitoring data, Landslides, 22, 2897–2914, https://doi.org/10.1007/s10346-024-02304-x, 2025b.

Hartmann, A. and Blume, T.: The evolution of hillslope hydrology: links between form, function and the underlying control of geology, Water Resour. Res., 60, e2023WR035937, https://doi.org/10.1029/2023WR035937, 2024.

Heisse, K., Roscher, C., Schumacher, J., and Schulze, E.-D.: Establishment of grassland species in monocultures: different strategies lead to success, Oecologia, 152, 435–447, https://doi.org/10.1007/s00442-007-0666-6, 2007.

Hong, H., Miao, Y., Liu, J., and Zhu, A.-X.: Exploring the effects of the design and quantity of absence data on the performance of random forest-based landslide susceptibility mapping, CATENA, 176, 45–64, https://doi.org/10.1016/j.catena.2018.12.035, 2019.

Hong, H., Wang, D., Zhu, A.-X., and Wang, Y.: Landslide susceptibility mapping based on the reliability of landslide and non-landslide sample, Expert Syst. Appl., 243, 122933, https://doi.org/10.1016/j.eswa.2023.122933, 2024.

Hong, Y., Adler, R., and Huffman, G.: Use of satellite remote sensing data in the mapping of global landslide susceptibility, Nat. Hazards, 43, 245–256, https://doi.org/10.1007/s11069-006-9104-z, 2007.

Huang, F., Cao, Z., Guo, J., Jiang, S.-H., Li, S., and Guo, Z.: Comparisons of heuristic, general statistical and machine learning models for landslide susceptibility prediction and mapping, CATENA, 191, 104580, https://doi.org/10.1016/j.catena.2020.104580, 2020.

Huang, F., Mao, D., Jiang, S.-H., Zhou, C., Fan, X., Zeng, Z., Catani, F., Yu, C., Chang, Z., Huang, J., Jiang, B., and Li, Y.: Uncertainties in landslide susceptibility prediction modeling: A review on the incompleteness of landslide inventory and its influence rules, Geosci. Front., 15, 101886, https://doi.org/10.1016/j.gsf.2024.101886, 2024.

Hungr, O., Leroueil, S., and Picarelli, L.: The Varnes classification of landslide types, an update, Landslides, 11, 167–194, https://doi.org/10.1007/s10346-013-0436-y, 2014.

Jaafari, A., Panahi, M., Pham, B. T., Shahabi, H., Bui, D. T., Rezaie, F., and Lee, S.: Meta optimization of an adaptive neuro-fuzzy inference system with grey wolf optimizer and biogeography-based optimization algorithms for spatial prediction of landslide susceptibility, CATENA, 175, 430–445, https://doi.org/10.1016/j.catena.2018.12.033, 2019.

Jacobs, L., Dewitte, O., Poesen, J., Maes, J., Mertens, K., Sekajugo, J., and Kervyn, M.: Landslide characteristics and spatial distribution in the Rwenzori Mountains, Uganda, J. Afr. Earth Sci., 134, 917–930, https://doi.org/10.1016/j.jafrearsci.2016.05.013, 2017.

Jones, J. N., Boulton, S. J., Bennett, G. L., Stokes, M., and Whitworth, M. R. Z.: Temporal variations in landslide distributions following extreme events: implications for landslide susceptibility modeling, J. Geophys. Res. Earth Surf., 126, e2021JF006067, https://doi.org/10.1029/2021JF006067, 2021.

Karger, D. N., Conrad, O., Böhner, J., Kawohl, T., Kreft, H., Soria-Auza, R. W., Zimmermann, N. E., Linder, H. P., and Kessler, M.: Climatologies at high resolution for the earth's land surface areas, Sci. Data, 4, 170122, https://doi.org/10.1038/sdata.2017.122, 2017.

https://doi.org/10.5194/egusphere-2026-2858
Preprint. Discussion started: 10 June 2026

Karsa, A., Punwani, S., and Shmueli, K.: The effect of low resolution and coverage on the accuracy of susceptibility mapping, Magn. Reson. Med., 81, 1833–1848, https://doi.org/10.1002/mrm.27542, 2019.

Kavzoglu, T., Teke, A., and Yilmaz, E. O.: Shared blocks-based ensemble deep learning for shallow landslide susceptibility mapping, Remote Sens., 13, 4776, https://doi.org/10.3390/rs13234776, 2021.

Kim, J.-C., Lee, S., Jung, H.-S., and Lee, S.: Landslide susceptibility mapping using random forest and boosted tree models in Pyeong-Chang, Korea, Geocarto Int., 33, 1000–1015, https://doi.org/10.1080/10106049.2017.1323964, 2018.

KOBO: Kompetenzzentrum Boden, https://ccsols.ch/de/home/, 2024.

Kosugi, K., Katsura, S., Katsuyama, M., and Mizuyama, T.: Water flow processes in weathered granitic bedrock and their effects on runoff generation in a small headwater catchment, Water Resour. Res., 42, https://doi.org/10.1029/2005WR004275, 2006.

Kruskal, W. H. and Wallis, W. A.: Use of ranks in one-criterion variance analysis, J. Am. Stat. Assoc., 47, 583–621, https://doi.org/10.1080/01621459.1952.10483441, 1952.

Lai, J.-S., Chiang, S.-H., and Tsai, F.: Exploring influence of sampling strategies on event-based landslide susceptibility modeling, ISPRS Int. J. Geo-Inf., 8, 397, https://doi.org/10.3390/ijgi8090397, 2019.

Lanni, C., McDonnell, J., Hopp, L., and Rigon, R.: Simulated effect of soil depth and bedrock topography on near-surface hydrologic response and slope stability, Earth Surf. Process. Landf., 38, 146–159, https://doi.org/10.1002/esp.3267, 2013.

Lee, S., Choi, J., and Woo, I.: The effect of spatial resolution on the accuracy of landslide susceptibility mapping: a case study in Boun, Korea, Geosci. J., 8, 51–60, https://doi.org/10.1007/BF02910278, 2004.

Lehner, B. and Grill, G.: Global river hydrography and network routing: baseline data and new approaches to study the world's large river systems, Hydrol. Process., 27, 2171–2186, https://doi.org/10.1002/hyp.9740, 2013.

Leonarduzzi, E. and Molnar, P.: Deriving rainfall thresholds for landsliding at the regional scale: daily and hourly resolutions, normalisation, and antecedent rainfall, Nat. Hazards Earth Syst. Sci., 20, 2905–2919, https://doi.org/10.5194/nhess-20-2905-2020, 2020.

Liechti, K., Badoux, A., Röthlisberger, G., Loat, R., and Bezzola, G. R.: 50 Jahre Erfassung von Unwetterschäden in der Schweiz, Wasser Energ. Luft, 114, 247–248, 2022.

Lima, P., Steger, S., Glade, T., and Murillo-García, F. G.: Literature review and bibliometric analysis on data-driven assessment of landslide susceptibility, J. Mt. Sci., 19, 1670–1698, https://doi.org/10.1007/s11629-021-7254-9, 2022.

Liu, S., Wang, L., Zhang, W., He, Y., and Pijush, S.: A comprehensive review of machine learning-based methods in landslide susceptibility mapping, Geol. J., 58, 2283–2301, https://doi.org/10.1002/gj.4666, 2023.

Liu, X.: Airborne LiDAR for DEM generation: some critical issues - Xiaoye Liu, 2008, Prog. Phys. Geogr., 32, 31–49, https://doi.org/10.1177/0309133308089496, 2008.

Lobo, J. M., Jiménez-Valverde, A., and Real, R.: AUC: a misleading measure of the performance of predictive distribution models, Glob. Ecol. Biogeogr., 17, 145–151, https://doi.org/10.1111/j.1466-8238.2007.00358.x, 2008.

https://doi.org/10.5194/egusphere-2026-2858
Preprint. Discussion started: 10 June 2026

Lombardo, L., Cama, M., Maerker, M., and Rotigliano, E.: A test of transferability for landslides susceptibility models under extreme climatic events: application to the Messina 2009 disaster, Nat. Hazards, 74, 1951–1989, https://doi.org/10.1007/s11069-014-1285-2, 2014.

Lu, N. and Godt, J. W.: Hillslope hydrology and stability, Cambridge University Press, 463 pp., ISBN: 978-1-139-61985-1, 2013.

Lu, N., Godt, J. W., and Wu, D. T.: A closed-form equation for effective stress in unsaturated soil, Water Resour. Res., 46, https://doi.org/10.1029/2009WR008646, 2010.

Ma, S., Shao, X., and Xu, C.: Landslide susceptibility mapping in terms of the slope-unit or raster-unit, which is better?, J. Earth Sci., 34, 386–397, https://doi.org/10.1007/s12583-021-1407-1, 2023.

Ma, Y., Minasny, B., Malone, B. P., and Mcbratney, A. B.: Pedology and digital soil mapping (DSM), Eur. J. Soil Sci., 70, 216–235, https://doi.org/10.1111/ejss.12790, 2019.

Ma, Z. and Chen, H. Y. H.: Effects of species diversity on fine root productivity increase with stand development and associated mechanisms in a boreal forest, J. Ecol., 105, 237–245, https://doi.org/10.1111/1365-2745.12667, 2017.

McDonnell, J. J.: Where does water go when it rains? Moving beyond the variable source area concept of rainfall-runoff response, Hydrol. Process., 17, 1869–1875, https://doi.org/10.1002/hyp.5132, 2003.

McGuire, L. A., Rengers, F. K., Kean, J. W., Coe, J. A., Mirus, B. B., Baum, R. L., and Godt, J. W.: Elucidating the role of vegetation in the initiation of rainfall-induced shallow landslides: Insights from an extreme rainfall event in the Colorado Front Range, Geophys. Res. Lett., 43, 9084–9092, https://doi.org/10.1002/2016GL070741, 2016.

Merghadi, A., Yunus, A. P., Dou, J., Whiteley, J., ThaiPham, B., Bui, D. T., Avtar, R., and Abderrahmane, B.: Machine learning methods for landslide susceptibility studies: A comparative overview of algorithm performance, Earth-Sci. Rev., 207, 103225, https://doi.org/10.1016/j.earscirev.2020.103225, 2020.

MeteoSwiss: Federal Office of Meteorology and Climatology MeteoSwiss Data, https://www.meteoswiss.admin.ch/, 2024.

Mirus, B. B., Jones, E. S., Baum, R. L., Godt, J. W., Slaughter, S., Crawford, M. M., Lancaster, J., Stanley, T., Kirschbaum, D. B., Burns, W. J., Schmitt, R. G., Lindsey, K. O., and McCoy, K. M.: Landslides across the USA: occurrence, susceptibility, and data limitations, Landslides, 17, 2271–2285, https://doi.org/10.1007/s10346-020-01424-4, 2020.

Miyata, S., Kosugi, K., Gomi, T., and Mizuyama, T.: Effects of forest floor coverage on overland flow and soil erosion on hillslopes in Japanese cypress plantation forests, Water Resour. Res., 45, W06402, https://doi.org/10.1029/2008WR007270, 2009.

Montgomery, D. R.: Road surface drainage, channel initiation, and slope instability, Water Resour. Res., 30, 1925–1932, https://doi.org/10.1029/94WR00538, 1994.

Montgomery, D. R. and Dietrich, W. E.: A physically based model for the topographic control on shallow landsliding, Water Resour. Res., 30, 1153–1171, https://doi.org/10.1029/93WR02979, 1994.

Moon, S., Formetta, G., Higa, J. T., Busti, R., Bellugi, D. G., Milledge, D. G., Ebel, B. A., and Dietrich, W. E.: Deep critical zone controls on shallow landslides, Proc. Natl. Acad. Sci., 123, e2524542123, https://doi.org/10.1073/pnas.2524542123, 2026.

https://doi.org/10.5194/egusphere-2026-2858
Preprint. Discussion started: 10 June 2026

Moos, C., Bebi, P., Graf, F., Mattli, J., Rickli, C., and Schwarz, M.: How does forest structure affect root reinforcement and susceptibility to shallow landslides?, Earth Surf. Process. Landf., 41, 951–960, https://doi.org/10.1002/esp.3887, 2016.

Moradi, S., Huisman, J. A., Class, H., and Vereecken, H.: The effect of bedrock topography on timing and location of landslide initiation using the local factor of safety concept, Water, 10, 1290, https://doi.org/10.3390/w10101290, 2018.

Moser, M.: Zur Prognose von Massenbewegungen, Eclogae Geol Helv, 90, 381–391, https://doi.org/ISSN 0012-9402, 1997.

Neuhäuser, B., Damm, B., and Terhorst, B.: GIS-based assessment of landslide susceptibility on the base of the Weights-of-Evidence model, Landslides, 9, 511–528, https://doi.org/10.1007/s10346-011-0305-5, 2012.

Nguyen, V. V., Pham, B. T., Vu, B. T., Prakash, I., Jha, S., Shahabi, H., Shirzadi, A., Ba, D. N., Kumar, R., Chatterjee, J. M., and Bui, D. T.: Hybrid machine learning approaches for landslide susceptibility modeling, Forests, 10, 157, https://doi.org/10.3390/f10020157, 2019.

Nohani, E., Moharrami, M., Sharafi, S., Khosravi, K., Pradhan, B., Pham, B. T., Lee, S., and M. Melesse, A.: Landslide susceptibility mapping using different GIS-based bivariate models, Water, 11, 1402, https://doi.org/10.3390/w11071402, 2019.

Oguz, E. A., Depina, I., and Thakur, V.: Effects of soil heterogeneity on susceptibility of shallow landslides, Landslides, 19, 67–83, https://doi.org/10.1007/s10346-021-01738-x, 2022.

Onda, Y., Komatsu, Y., Tsujimura, M., and Fujihara, J.: The role of subsurface runoff through bedrock on storm flow generation, Hydrol. Process., 15, 1693–1706, https://doi.org/10.1002/hyp.234, 2001.

Palamakumbure, D., Flentje, P., and Stirling, D.: Consideration of optimal pixel resolution in deriving landslide susceptibility zoning within the Sydney Basin, New South Wales, Australia, Comput. Geosci., 82, 13–22, https://doi.org/10.1016/j.cageo.2015.05.002, 2015.

Peres, D. J. and Cancelliere, A.: Estimating return period of landslide triggering by Monte Carlo simulation, J. Hydrol., 541, 256–271, https://doi.org/10.1016/j.jhydrol.2016.03.036, 2016.

Perron, J. T.: Climate and the pace of erosional landscape evolution, Annu. Rev. Earth Planet. Sci., 45, 561–591, https://doi.org/10.1146/annurev-earth-060614-105405, 2017.

Persichillo, M. G., Bordoni, M., Meisina, C., Bartelletti, C., Barsanti, M., Giannecchini, R., D'Amato Avanzi, G., Galanti, Y., Cevasco, A., Brandolini, P., and Galve, J. P.: Shallow landslides susceptibility assessment in different environments, Geomat. Nat. Hazards Risk, 8, 748–771, https://doi.org/10.1080/19475705.2016.1265011, 2017.

Petschko, H., Brenning, A., Bell, R., Goetz, J., and Glade, T.: Assessing the quality of landslide susceptibility maps – case study Lower Austria, Nat. Hazards Earth Syst. Sci., 14, 95–118, https://doi.org/10.5194/nhess-14-95-2014, 2014.

Piacentini, D., Troiani, F., Soldati, M., Notarnicola, C., Savelli, D., Schneiderbauer, S., and Strada, C.: Statistical analysis for assessing shallow-landslide susceptibility in South Tyrol (south-eastern Alps, Italy), Geomorphology, 151–152, 196–206, https://doi.org/10.1016/j.geomorph.2012.02.003, 2012.

Piacentini, D., Devoto, S., Mantovani, M., Pasuto, A., Prampolini, M., and Soldati, M.: Landslide susceptibility modeling assisted by Persistent Scatterers Interferometry (PSI): an example from the northwestern coast of Malta, Nat. Hazards, 78, 681–697, https://doi.org/10.1007/s11069-015-1740-8, 2015.

https://doi.org/10.5194/egusphere-2026-2858
Preprint. Discussion started: 10 June 2026

Poggio, L., de Sousa, L. M., Batjes, N. H., Heuvelink, G. B. M., Kempen, B., Ribeiro, E., and Rossiter, D.: SoilGrids 2.0: producing soil information for the globe with quantified spatial uncertainty, SOIL, 7, 217–240, https://doi.org/10.5194/soil-7-217-2021, 2021.

Pourghasemi, H. R. and Rahmati, O.: Prediction of the landslide susceptibility: Which algorithm, which precision?, CATENA, 162, 177–192, https://doi.org/10.1016/j.catena.2017.11.022, 2018.

Pourghasemi, H. R., Jirandeh, A. G., Pradhan, B., Xu, C., and Gokceoglu, C.: Landslide susceptibility mapping using support vector machine and GIS at the Golestan Province, Iran, J. Earth Syst. Sci., 122, 349–369, https://doi.org/10.1007/s12040-013-0282-2, 2013.

Pourghasemi, H. R., Kornejady, A., Kerle, N., and Shabani, F.: Investigating the effects of different landslide positioning techniques, landslide partitioning approaches, and presence-absence balances on landslide susceptibility mapping, CATENA, 187, 104364, https://doi.org/10.1016/j.catena.2019.104364, 2020.

Ray, R. L., Jacobs, J. M., and Ballestero, T. P.: Regional landslide susceptibility: spatiotemporal variations under dynamic soil moisture conditions, Nat. Hazards, 59, 1317–1337, https://doi.org/10.1007/s11069-011-9834-4, 2011.

R-Core-Team: A language and environment for statistical computing, R Foundation for Statistical Computing (4.4.1), Vienna, Austria, https://www.R-project.org/, 2020.

Reichenbach, P., Rossi, M., Malamud, B. D., Mihir, M., and Guzzetti, F.: A review of statistically-based landslide susceptibility models, Earth-Sci. Rev., 180, 60–91, https://doi.org/10.1016/j.earscirev.2018.03.001, 2018.

Rickli, C.: Vegetationswirkungen und Rutschungen – Untersuchung zum Einfluss der Vegetation auf oberflächennahe Rutschprozesse anhand der Unwetterereignisse in Sachseln OW am 15. August 1997, Eidg. Forschungsanstalt WSL, Bundesamt für Umwelt, Wald und Landschaft, Birmensdorf, Bern, 2001.

Rickli, C., McArdell, B., Badoux, A., and Loup, B.: Database shallow landslides and hillslope debris flows, in: Proceedings of the 13th Congress INTERPRAEVENT, 242–243, https://hangmuren.wsl.ch/, 2016.

Rickli, C., Graf, F., Bebi, P., Bast, A., Loup, B., and McArdell, B.: Schützt der Wald vor Rutschungen? Hinweise aus der WSL-Rutschungsdatenbank, Schweiz. Z. Forstwes., 170, 310–317, https://doi.org/10.3188/szf.2019.0310, 2019.

Ripley, B. D.: Pattern Recognition and Neural Networks, Cambridge University Press, 420 pp., ISBN: 978-0-521-71770-0, 2007.

Roda-Boluda, D. C., D'Arcy, M., McDonald, J., and Whittaker, A. C.: Lithological controls on hillslope sediment supply: insights from landslide activity and grain size distributions, Earth Surf. Process. Landf., 43, 956–977, https://doi.org/10.1002/esp.4281, 2018.

Roering, J. J., Schmidt, K. M., Stock, J. D., Dietrich, W. E., and Montgomery, D. R.: Shallow landsliding, root reinforcement, and the spatial distribution of trees in the Oregon Coast Range, Can. Geotech. J., 40, 237–253, https://doi.org/10.1139/t02-113, 2003.

Rossi, G., Catani, F., Leoni, L., Segoni, S., and Tofani, V.: HIRESSS: a physically based slope stability simulator for HPC applications, Nat. Hazards Earth Syst. Sci., 13, 151–166, https://doi.org/10.5194/nhess-13-151-2013, 2013.

Rossi, M., Guzzetti, F., Reichenbach, P., Mondini, A. C., and Peruccacci, S.: Optimal landslide susceptibility zonation based on multiple forecasts, Geomorphology, 114, 129–142, https://doi.org/10.1016/j.geomorph.2009.06.020, 2010.

https://doi.org/10.5194/egusphere-2026-2858
Preprint. Discussion started: 10 June 2026

von Ruette, J., Papritz, A., Lehmann, P., Rickli, C., and Or, D.: Spatial statistical modeling of shallow landslides—Validating predictions for different landslide inventories and rainfall events, Geomorphology, 133, 11–22, https://doi.org/10.1016/j.geomorph.2011.06.010, 2011.

Schad, P.: World Reference Base for Soil Resources—Its fourth edition and its history, J. Plant Nutr. Soil Sci., 186, 151–163, https://doi.org/10.1002/jpln.202200417, 2023.

Schmidt, K. M., Roering, J. J., Stock, J. D., Dietrich, W. E., Montgomery, D. R., and Schaub, T.: The variability of root cohesion as an influence on shallow landslide susceptibility in the Oregon Coast Range, Can. Geotech. J., 38, 995–1024, https://doi.org/10.1139/t01-031, 2001.

Schwarz, M., Cohen, D., and Or, D.: Pullout tests of root analogs and natural root bundles in soil: Experiments and modeling, J. Geophys. Res. Earth Surf., 116, https://doi.org/10.1029/2010JF001753, 2011.

Selby, M. J.: Controls on the stability and inclinations of hillslopes formed on hard rock, Earth Surf. Process. Landf., 7, 449–467, https://doi.org/10.1002/esp.3290070506, 1982.

Shano, L., Raghuvanshi, T. K., and Meten, M.: Landslide susceptibility evaluation and hazard zonation techniques – a review, Geoenvironmental Disasters, 7, 18, https://doi.org/10.1186/s40677-020-00152-0, 2020.

Sidle, R. and Ochiai, H.: Landslides: Processes, Prediction, and Land Use, Water Resour. Monogr. Am. Geophys. Union Wash., 525, https://doi.org/10.1029/WM018, 2006.

Sidle, R. C. and Bogaard, T. A.: Dynamic earth system and ecological controls of rainfall-initiated landslides, Earth-Sci. Rev., 159, 275–291, https://doi.org/10.1016/j.earscirev.2016.05.013, 2016.

Steger, S., Brenning, A., Bell, R., Petschko, H., and Glade, T.: Exploring discrepancies between quantitative validation results and the geomorphic plausibility of statistical landslide susceptibility maps, Geomorphology, 262, 8–23, https://doi.org/10.1016/j.geomorph.2016.03.015, 2016a.

Steger, S., Brenning, A., Bell, R., and Glade, T.: The propagation of inventory-based positional errors into statistical landslide susceptibility models, Nat. Hazards Earth Syst. Sci., 16, 2729–2745, https://doi.org/10.5194/nhess-16-2729-2016, 2016b.

Steger, S., Brenning, A., Bell, R., and Glade, T.: The influence of systematically incomplete shallow landslide inventories on statistical susceptibility models and suggestions for improvements, Landslides, 14, 1767–1781, https://doi.org/10.1007/s10346-017-0820-0, 2017.

Sun, D., Gu, Q., Wen, H., Xu, J., Zhang, Y., Shi, S., Xue, M., and Zhou, X.: Assessment of landslide susceptibility along mountain highways based on different machine learning algorithms and mapping units by hybrid factors screening and sample optimization, Gondwana Res., 123, 89–106, https://doi.org/10.1016/j.gr.2022.07.013, 2023.

Swisstopo: swissALTI3D -Das hoch aufgelöste Terrainmodell der Schweiz: https://www.swisstopo.admin.ch/en/height-model-swissalti3d, last access: 3 March 2025a.

Swisstopo: GeoCover: https://www.swisstopo.admin.ch/en/geological-model-2d-geocover, last access: 27 February 2025b.

Swisstopo: SWISSIMAGE: https://www.swisstopo.admin.ch/en/orthoimage-swissimage-10, last access: 23 February 2025c.

https://doi.org/10.5194/egusphere-2026-2858
Preprint. Discussion started: 10 June 2026

Swisstopo: swissTLM3D - Topographic Landscape Model: https://www.swisstopo.admin.ch/en/landscape-model-swisstlm3d, last access: 10 January 2025d.

Taalab, K., Cheng, T., and Zhang, Y.: Mapping landslide susceptibility and types using Random Forest, Big Earth Data, 2, 159–178, https://doi.org/10.1080/20964471.2018.1472392, 2018.

Terzaghi, K.: Theoretical soil mechanics, John Wiley and Sons, London, 1943.

Thornton, P. E., Running, S. W., and White, M. A.: Generating surfaces of daily meteorological variables over large regions of complex terrain, J. Hydrol., 190, 214–251, https://doi.org/10.1016/S0022-1694(96)03128-9, 1997.

Titti, G., van Westen, C., Borgatti, L., Pasuto, A., and Lombardo, L.: When enough is really enough? on the minimum number of landslides to build reliable susceptibility models, Geosciences, 11, 469, https://doi.org/10.3390/geosciences11110469, 2021.

Uchida, T.: Clarifying the role of pipe flow on shallow landslide initiation, Hydrol. Process., 18, 375–378, https://doi.org/10.1002/hyp.5214, 2004.

Uchida, T., Kosugi, K., and Mizuyama, T.: Effects of pipeflow on hydrological process and its relation to landslide: a review of pipeflow studies in forested headwater catchments, Hydrol. Process., 15, 2151–2174, https://doi.org/10.1002/hyp.281, 2001.

Unesco: International classification and mapping of vegetation, Unesco, Paris, 101 pp., 1973.

UniGeneva: Normalized Difference Vegetation Index (NDVI) - Annual Mean - Switzerland, https://doi.org/10.26037/yareta:kpmscrogqbdhvjeuev2ydrzk7y, 2019.

Vallejo, L. E.: Interpretation of the limits in shear strength in binary granular mixtures, Can. Geotech. J., https://doi.org/10.1139/t01-029, 2011.

Večeřa, M., Divíšek, J., Lenoir, J., Jiménez-Alfaro, B., Biurrun, I., Knollová, I., Agrillo, E., Campos, J. A., Čarni, A., Crespo Jiménez, G., Ćuk, M., Dimopoulos, P., Ewald, J., Fernández-González, F., Gégout, J.-C., Indreica, A., Jandt, U., Jansen, F., Kącki, Z., Rašomavičius, V., Řezníčková, M., Rodwell, J. S., Schaminée, J. H. J., Šilc, U., Svenning, J.-C., Swacha, G., Vassilev, K., Venanzoni, R., Willner, W., Wohlgemuth, T., and Chytrý, M.: Alpha diversity of vascular plants in European forests, J. Biogeogr., 46, 1919–1935, https://doi.org/10.1111/jbi.13624, 2019.

Wang, L. and Liu, H.: An efficient method for identifying and filling surface depressions in digital elevation models for hydrologic analysis and modelling, Int. J. Geogr. Inf. Sci., 20, 193–213, https://doi.org/10.1080/13658810500433453, 2006.

van Westen, C. J., Castellanos, E., and Kuriakose, S. L.: Spatial data for landslide susceptibility, hazard, and vulnerability assessment: An overview, Eng. Geol., 102, 112–131, https://doi.org/10.1016/j.enggeo.2008.03.010, 2008.

Wicki, A., Lehmann, P., Hauck, C., Seneviratne, S. I., Waldner, P., and Stähli, M.: Assessing the potential of soil moisture measurements for regional landslide early warning, Landslides, 17, 1881–1896, https://doi.org/10.1007/s10346-020-01400-y, 2020.

Woodard, J. B., Mirus, B. B., Crawford, M. M., Or, D., Leshchinsky, B. A., Allstadt, K. E., and Wood, N. J.: Mapping landslide susceptibility over large regions with limited data, J. Geophys. Res. Earth Surf., 128, e2022JF006810, https://doi.org/10.1029/2022JF006810, 2023.

https://doi.org/10.5194/egusphere-2026-2858
Preprint. Discussion started: 10 June 2026

Zevenbergen, L. W. and Thorne, C. R.: Quantitative analysis of land surface topography, Earth Surf. Process. Landf., 12, 47–56, https://doi.org/10.1002/esp.3290120107, 1987.

Zêzere, J., Henriques, C., Garcia, R., Oliveira, S., and Piedade, A.: Effects of landslide inventories uncertainty on landslide susceptibility modelling, in: Landslide Processes: From Geomorphologic Mapping to Dynamic Modelling, CERG Editions, Strasbourg, 81–86, 2009.

Zhang, Q., Shao, M., Jia, X., and Zhang, C.: Understory vegetation and drought effects on soil aggregate stability and aggregate-associated carbon on the loess plateau in China, Soil Sci. Soc. Am. J., 82, 106–114, https://doi.org/10.2136/sssaj2017.05.0145, 2018.

Zhao, X., Zhao, Z., Huang, F., Huang, J., Yang, Z., Chen, Q., Zhou, D., Fang, L., Ye, X., and Chao, J.: Application of environmental variables in statistically-based landslide susceptibility mapping: A review, Front. Earth Sci., 11, https://doi.org/10.3389/feart.2023.1147427, 2023.

Zhu, Q., Chen, L., Hu, H., Pirasteh, S., Li, H., and Xie, X.: Unsupervised feature learning to improve transferability of landslide susceptibility representations, IEEE J. Sel. Top. Appl. Earth Obs. Remote Sens., 13, 3917–3930, https://doi.org/10.1109/JSTARS.2020.3006192, 2020.

Zweifel, L., Samarin, M., Meusburger, K., and Alewell, C.: Investigating causal factors of shallow landslides in grassland regions of Switzerland, Nat. Hazards Earth Syst. Sci., 21, 3421–3437, https://doi.org/10.5194/nhess-21-3421-2021, 2021.